**Cluster Dynamics-based Parameterization for Sulfuric Acid-Dimethylamine Nucleation: Comparison and Selection through Box- and Three-Dimensional-Modeling**

Jiewen Shen[1,2], Bin Zhao[1,2], Shuxiao Wang[1,2,*], An Ning[3], Yuyang Li[2], Runlong Cai[4], Da Gao[1,2], Biwu Chu[5,6], Yang Gao[7], Manish Shrivastava[8], Jingkun Jiang[2], Xiuhui Zhang[3], Hong He[5,6]

[1]*State Key Joint Laboratory of Environment Simulation and Pollution Control, School of Environment, Tsinghua University, Beijing, 100084, China*

[2]*State Environmental Protection Key Laboratory of Sources and Control of Air Pollution Complex, Beijing, 100084, China*

[3]*Key Laboratory of Cluster Science, Ministry of Education of China, School of Chemistry and Chemical Engineering, Beijing Institute of Technology, Beijing, 100081, China*

[4]*Shanghai Key Laboratory of Atmospheric Particle Pollution and Prevention (LAP³), Department of Environmental Science & Engineering, Fudan University, Shanghai, 200438, China*

[5]*State Key Joint Laboratory of Environment Simulation and Pollution Control, Research Center for Eco-Environmental Sciences, Chinese Academy of Sciences, Beijing 100085, China*

[6]*College of Resources and Environment, University of Chinese Academy of Sciences, Beijing 100049, China*

[7]*Key Laboratory of Marine Environment and Ecology, Ministry of Education, Ocean University of China, Qingdao 266100, China*

[8]*Pacific Northwest National Laboratory, Richland, Washington, USA*

*Correspondence to: Shuxiao Wang (shxwang@tsinghua.edu.cn)

Formatted: Justified

**ABSTRACT**

Clustering of gaseous sulfuric acid (SA) enhanced by dimethylamine (DMA) is a major mechanism for new particle formation (NPF) in polluted atmospheres. However, uncertainty remains regarding the SA-DMA nucleation parameterization that reasonably represents cluster dynamics and is applicable across various atmospheric conditions. This uncertainty hinders accurate three-dimensional (3-D) modeling of NPF and subsequent assessment of its environmental and climatic impacts. Here we extensively compare different cluster dynamics-based parameterizations for SA-DMA nucleation and identify the most reliable one through a combination of box-model simulations, 3-D modeling, and in-situ observations. Results show that the parameterization derived from Atmospheric Cluster Dynamic Code (ACDC) simulations, incorporating the latest theoretical insights (DLPNO-CCSD(T)/aug-cc-pVTZ//ωB97X-D/6-311++G(3df,3pd) level of theory) and adequate representation of cluster dynamics, exhibits dependable performance in 3-D NPF simulation for both winter and summer conditions in Beijing and shows promise for application in diverse atmospheric conditions. Another ACDC-derived parameterization, replacing the level of theory with RI-CC2/aug-cc-pV(T+d)Z//M06-2X/6–311++G(3df,3pd), also performs well in NPF modeling at relatively low temperatures around 280 K but exhibits limitations at higher temperatures due to inappropriate representation of SA-DMA cluster thermodynamics. Additionally, a previously reported parameterization incorporating simplifications is applicable for simulating NPF in polluted atmospheres but tends to overestimate particle formation rates under conditions of elevated temperature (> ~300 K) and low condensation sink (< ~3×10$^{-3}$ s$^{-1}$). Our findings highlight the applicability of the new ACDC-derived parameterization, which couples the latest SA-DMA nucleation theory and holistic cluster dynamics, in 3-D NPF modeling. The ACDC-derived parameterization framework provides valuable reference for developing parameterizations for other nucleation systems.

55  **GRAPHICAL ABSTRACT**

56
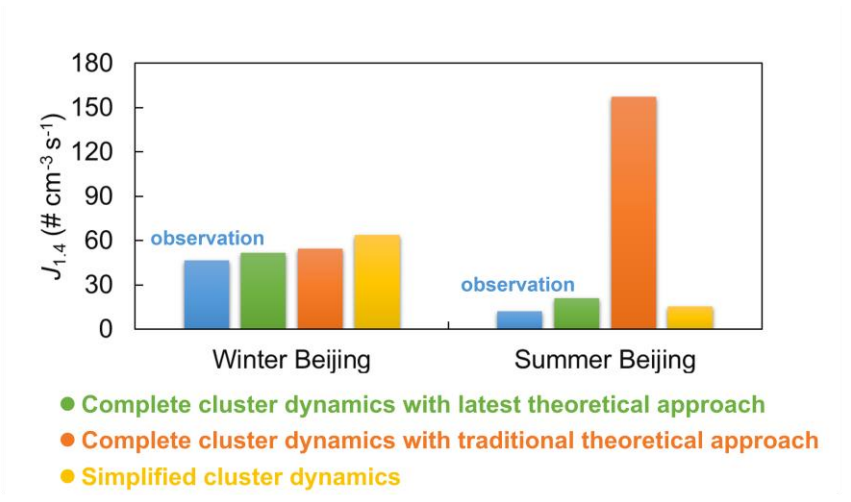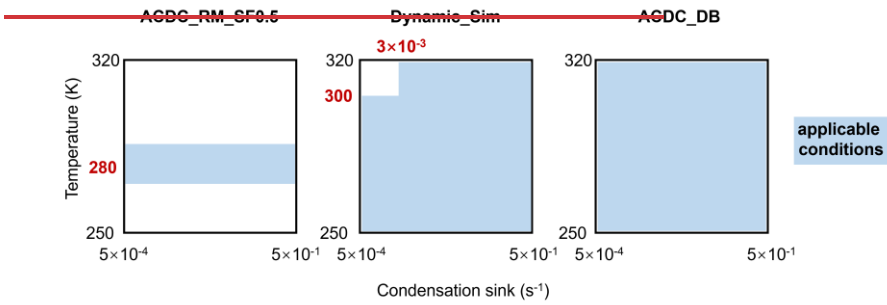
ACDC_RM_SF0.5:
  ACDC-derived parameterization with traditional theoretical approach
Dynamic_Sim:
  reported parameterization with simplifications in cluster dynamics
ACDC_DB:
  ACDC-derived parameterization with latest theoretical approach

58

59

## 1 INTRODUCTION

Atmospheric aerosols have significant impacts on visibility, human health, and global climate (Gordon et al., 2016; Gao et al., 2024). New Particle Formation (NPF) is the predominant source of global aerosol population, with nucleation being the key stage of the gas-to-particle transformation (Zhao et al., 2020; Almeida et al., 2013). In polluted regions such as urban China, compelling evidence indicates that sulfuric acid (SA)-driven nucleation enhanced by dimethylamine (DMA) can generate thermodynamically stable SA-DMA clusters and lead to high particle formation rates close to kinetic limit of SA clustering, which is responsible for the observed intensive NPF events (Cai et al., 2021; Yao et al., 2018). Meanwhile, it has been demonstrated that variations in atmospheric conditions, including condensation sinks (CS) arising from background aerosols, along with temperature ($T$), can exert profound impacts on the cluster dynamics of SA-DMA nucleation by varying the particle formation rates across several orders of magnitude (Cai et al., 2021; Deng et al., 2020). Given that complex interactions exist among various gaseous precursors, molecular clusters, and pre-existing aerosols during nucleation, reasonable representation of the cluster dynamics of SA-DMA nucleation in three-dimensional (3-D) models is important for 3-D NPF modeling and subsequent assessment of its impacts on environment and climate.

Empirical models in form of power law functions have been extensively utilized to examine how particle formation rates respond to precursor concentrations (Semeniuk and Dastoor, 2018). Through parameter fitting, these empirical models can effectively reproduce the particle formation rates observed in both laboratory experiments and field measurements (Kulmala et al., 2006; Riccobono et al., 2014; Semeniuk and Dastoor, 2018). Subsequently, they can be integrated into 3-D models for regional or global NPF simulations. Bergman et al. (2015) and Dunne et al. (2016) have simulated SA-DMA nucleation utilizing global models, which incorporate empirical equations derived from experimental data obtained from CLOUD chamber or flow tube experiments. These parameterization schemes successfully characterize the response of particle formation rates to precursor concentrations, however, they fail to account for dependencies on $T$ and CS due to the ignorance of explicit cluster dynamics. As a result, they are identified to be inadequate for accurately reproducing NPF events in winter Beijing (Li et al., 2023c).

We recently developed an analytical equation for SA-DMA nucleation parameterization based on detailed cluster dynamics simulations (abbreviated as Dynamic_Sim) (Li et al., 2023c). Previous theoretical insights into the SA-DMA system (Olenius et al., 2013, 2017; Ortega et al., 2012; Myllys et al., 2019) indicate that $(SA)_k(DMA)_k$ ($k$ = 1-4) and $(SA)_2(DMA)_1$ clusters are considered the key clusters along the cluster formation pathways in SA-DMA nucleation. Under the polluted conditions (CS > ~$1.0\times10^{-2}$ s$^{-1}$), the evaporation rates of clusters $(SA)_k(DMA)_k$ ($k$ = 2-4) and $(SA)_2(DMA)_1$ clusters are negligible compared to their coagulation sink. Accordingly~~To derive an explicit equation~~, several simplifications have been made in

102 Dynamic_Sim, including 1) only $(SA)_k(DMA)_k$ ($k$ = 1-4) and $(SA)_2(DMA)_1$ clusters are
103 considered; 2) clusters larger than $(SA)_1(DMA)_1$ are regarded stable with no
104 evaporation; and 3) $(SA)_4(DMA)_4$ cluster is the only terminal cluster in calculating
105 particle formation rates. Subsequent applications in 3-D modeling have demonstrated
106 significantly improved performance of Dynamic_Sim compared to previous data-fitting
107 parameterizations in simulating the particle formation rates, the evolution of particle
108 number size distributions (PNSDs), and NPF events in winter Beijing. However, the
109 efficacy of Dynamic_Sim in NPF simulation has yet to be assessed under varying
110 atmospheric conditions, such as the summer season characterized by relatively higher
111 $T$ and lower CS compared to winter. Moreover, the impacts of simplifications made in
112 the derivation of Dynamic_Sim on 3-D NPF simulation under different atmospheric
113 conditions remain unclear.
114 In addition to the form of explicit formulations, integration of nucleation dynamics
115 in 3-D models can also be realized using precomputed look-up tables generated by box
116 models. Atmospheric Cluster Dynamics Code (ACDC) is a representativeflexible box
117 model for simulating cluster dynamics and particle formation rates (Mcgrath et al., 2012;
118 Olenius et al, 2013). In addition to representing $T$- and CS- dependencies for particle
119 formation rate as Dynamic_Sim, ACDC considers the source/sink terms of all given
120 molecules/clusters within a nucleation system without simplifications of the clustering
121 processes. By integrating quantum chemical calculations with ACDC, Almeida et al.
122 (2013) discovered that the simulated SA-DMA nucleation provides valuable insights
123 for interpreting the measurements from the CLOUD chamber experiments. Similarly,
124 Lu et al. (2020) demonstrated that ACDC coupled with quantum chemistry calculations
125 can effectively reproduce the particle formation rates observed in urban Shanghai. In
126 addition to its extensive utilization in box modeling (Almeida et al., 2013; Lu et al.,
127 2020; Yang et al., 2021), several studies have simulated nucleation pathways in
128 chemical transport models using precomputed look-up tables generated by ACDC. For
129 example, Baranizadeh et al. (2016) and Croft et al. (2016) used ACDC-derived look-up
130 tables as nucleation parameterizations to probe the impacts of SA–$NH_3$–$H_2O$ nucleation
131 on aerosol number concentration, cloud properties, and radiation balance. Olin et al.
132 (2022) and Julin et al. (2018) evaluated the impact of new particle formation on aerosol
133 number concentrations in Europe under historical and emission reduction scenarios,
134 respectively, using ACDC-derived parameterizations involving both SA–$NH_3$–$H_2O$ and
135 SA-DMA nucleation. It should be noted thatWhile ACDC has been extensively utilized
136 in box modeling (Almeida et al., 2013; Lu et al., 2020; Yang et al., 2021), its potential
137 for deriving parameterizations for 3-D models has not been explored in previous studies.
138 Furthermore, ACDC program in modeling the nucleation process is highly reliant on
139 specific thermodynamic data for the molecular clusters of interest, which are primarily
140 obtained through quantum chemical calculations (Elm et al., 2020). A very recent study
141 by Svenhag et al. (2024) compared the impact of two typical quantum calculation
142 methods on 3-D modeling of SA-$NH_3$ nucleation using ACDC-derived
143 parameterizations. However, it is still unclear how different quantum chemical methods

144 affect the 3-D modeling of SA-DMA nucleation. ~~The uncertainty surrounding the~~
145 ~~influence of different quantum chemical calculation approaches adds additional~~
146 ~~complexity to the application of ACDC-derived parameterization in 3-D NPF modeling.~~
147      This study aims to compare different cluster dynamic-based parameterizations for
148 SA-DMA nucleation and identify the robust one applicable for 3-D models. We
149 introduced ~~new~~ parameterizations developed using the ACDC program, incorporating
150 various quantum chemical calculations. Different cluster dynamic-based
151 parameterizations, including ACDC-derived ones as well as Dynamic_Sim, are
152 comprehensively compared and evaluated through a combination of box-model
153 simulations, 3-D modeling, and in-situ observational data. Our findings reveal that by
154 incorporating the latest theoretical understanding and complete representation of cluster
155 dynamics, ACDC-derived parameterization demonstrates reliable performance in 3-D
156 NPF simulation for both winter and summer conditions in Beijing and exhibits potential
157 applicability in diverse atmospheric conditions. The study sheds light on the impacts of
158 employing various simplifications in cluster dynamics and different theoretical
159 approaches in deriving parameterizations on NPF simulation. In addition to
160 contributing to the precise simulation of SA-DMA nucleation and the quantification of
161 its environmental and climatic effects, this study provides valuable references for
162 simulating other nucleation mechanisms in 3-D models.
163 **2 METHODS**
164 **2.1 Configurations of ACDC**
165      Here, $(SA)_m(DMA)_n$ clusters ($0 < n \leq m \leq 3$, $m$ and $n$ represent the number of
166 SA and DMA molecules in a cluster) are used to build the ACDC-derived
167 parameterizations for SA-DMA nucleation due to their reported much higher stability
168 compared to those containing more DMA molecules than SA molecules (Xie et al.,
169 2017). The ACDC code is available at https://github.com/tolenius/ACDC. ~~2017).~~ The
170 conformations and thermodynamics of SA-DMA clusters are taken from our other
171 study (Ning et al., 2024). Briefly, the conformations of selected clusters are taken from
172 the reported global minima from Li et al. (2020), and the key thermodynamic data for
173 ACDC, Gibbs free energy change ($\Delta G$), are recalculated at the DLPNO-CCSD(T)/aug-
174 cc-pVTZ//$\omega$B97X-D/6-311++G(3df,3pd) level of theory. Based on benchmark studies
175 (Elm et al., 2020), this level of theory provides dependable thermodynamic insights into
176 molecular clusters during nucleation and represents the latest theoretical approach. In
177 addition, the rotational symmetry is consistently considered in quantum calculations
178 following Besel et al. (2020). Following most previous ACDC simulation studies (Xie
179 et al., 2017; Elm et al., 2020; Ning et al., 2020), $(SA)_4(DMA)_3$ and $(SA)_4(DMA)_4$
180 clusters are defined as the boundary conditions, i.e. the clusters fluxing out the
181 simulated system and participating in subsequent growth in ACDC simulations,
182 considering their high stability. Since clusters containing SA tetramers are estimated to
183 have an electrical mobility diameter of 1.4 nm (Cai et al., 2023; Jen et al., 2014; Thomas
184 et al., 2016), the formation rates of $(SA)_4(DMA)_3$ and $(SA)_4(DMA)_4$ clusters are
185 therefore deemed as the particle formation rates at 1.4 nm ($J_{1.4}$). Size-dependent

186 coagulation sink (CoagS) is counted for each SA-DMA cluster which is consistent with
187 Dynamic_Sim (Li et al., 2023c):

$$\text{CoagS}_i = \text{CS} \left(\frac{V_i}{V_1}\right)^{-\frac{1.7}{3}}$$

189 where $V_i$ and $V_1$ (m$^3$) represent the volume of cluster $i$ and SA molecule, respectively.
190 The power-law exponent of -1.7 is selected according to typical range in the atmosphere
191 (Lehtinen et al., 2007). In addition, enhancement for collision processes from Van de
192 Waals forces is also considered. We refer to the ACDC-derived parameterization in
193 coupling the DLPNO-CCSD(T)/aug-cc-pVTZ//ωB97X-D/6-311++G(3df,3pd) level of
194 theory and adequate cluster dynamics as ACDC_DB, which is established as the base-
195 case for our discussion of other cluster dynamics-based parameterizations.
196     In addition to the direct comparison of ACDC_DB to Dynamic_Sim, additional test
197 parameterizations combining ACDC_DB and three simplifications within
198 Dynamic_Sim are established and compared with ACDC_DB to further probe the
199 impacts of these simplifications on NPF simulations. According to our previous study,
200 altering the simplifications within Dynamic_Sim to explicit treatment would
201 substantially escalate the computational demand by several orders of magnitude (Li et
202 al. 2023c). Therefore, we utilize the ACDC-derived look-up tables to evaluate the
203 impacts of the simplified treatments. The configurations of all parameterizations are
204 detailed in Table 1. It should be noted that when all simplifications are applied on
205 ACDC_DB, Dynamic_Sim still predicts higher $J_{1.4}$ compared to ACDC_DB (Figure
206 S1A). This is because the $\Delta G$ value of the initial (SA)$_1$(DMA)$_1$ cluster at 298.15 K used
207 in Dynamic_Sim, which is taken from Myllys et al. (Myllys et al., 2019), is slightly
208 lower than that used in ACDC_DB (-13.5 kcal mol$^{-1}$ for Dynamic_Sim and -12.9 kcal
209 mol$^{-1}$ for ACDC_DB) (Ning et al., 2024), even though both parameterizations employ
210 the quantum chemical calculation method of DLPNO-CCSD(T). Possible reasons for
211 the discrepancy include the utilization of a larger basis set (3-zeta 6-311++G(3df,3pd))
212 and higher convergence criteria (Tight PNO + Tight SCF) in this study compared to
213 that in Myllys et al.. Aligning the $\Delta G$ for (SA)$_1$(DMA)$_1$ cluster in Dynamic_Sim with
214 that of ACDC leads to a high consistency in the predicted $J_{1.4}$ between the two
215 approaches (Figure S1B). The uncertainty of $\Delta G$ used in Dynamic_Sim is discussed in
216 our previous study (Li et al., 2023c) and here we mainly focus on the impacts of
217 simplifications in Dynamic_Sim.
218     While the DLPNO-CCSD(T)/aug-cc-pVTZ//ωB97X-D/6-311++G(3df,3pd) level
219 of theory yields reasonable cluster thermodynamics, quantum chemistry calculations
220 employing the RI-CC2 method predicting lower $\Delta G$ for cluster formation (stronger
221 binding between molecules within clusters), has been widely used in conjunction with
222 ACDC to interpret experimental and observed particle formation rates in previous
223 studies (Almeida et al., 2013; Kürten et al., 2018; Ning et al., 2020). The prevalent
224 combination used with the RI-CC2 method is RI-CC2/aug-cc-pV(T+d)Z//M06-2X/6-
225 311++G(3df,3pd) level of theory (Lu et al., 2020; Liu et al., 2021; Ning et al., 2022;
226 Ning and Zhang, 2022; Liu et al., 2019). Based on Elm's work, compared to DLPNO-

227  CCSD(T)/aug-cc-pVTZ//ωB97X-D/6-311++G(3df,3pd), the differences in predicted
228  cluster binding energies primarily stem from discrepancies between DLPNO-CCSD(T)
229  and RI-CC2 in single-point energy calculations, while the ωB97X-D and M06-2X
230  functionals exhibit similar performance (Elm et al., 2013; Elm et al., 2020). Also, in
231  previous studies the RI-CC2 method combined with ACDC was consistently
232  accompanied by application of a sticking factor (SF) of 0.5 in treating collision
233  processes (Almeida et al., 2013; Lu et al., 2020). However, it is noteworthy that,
234  according to Stolzenburg et al.'s's work (Stolzenburg et al., 2020), the SF of the neutral
235  SA-DMA cluster system should be unity. Here, we refer to the traditional theoretical
236  approach as employing the RI-CC2/aug-cc-pV(T+d)Z//M06-2X/6-311++G(3df,3pd)
237  level of theory and incorporating the SF of 0.5 in collision processes. An ACDC-derived
238  parameterization coupling the traditional theoretical approach is established to assess
239  the effectiveness of the traditional method in NPF simulation (ACDC_RM_SF0.5).
240  Except for the varied thermodynamic inputs and SF, the remaining configurations of
241  ACDC_RM_SF0.5 are identical to ACDC_DB. Additionally, we establish a test
242  parameterization coupling RI-CC2/aug-cc-pV(T+d)Z//M06-2X/6-311++G(3df,3pd)
243  level of theory with an SF of unity (ACDC_RM) to evaluate the impact solely arising
244  from the quantum chemical calculation method. Note that SF of unity is applied to all
245  parameterizations in this study except for the ACDC_RM_SF0.5.

246  To quantify the differences in simulating $J_{1.4}$ among different cluster dynamics-
247  based parameterizations compared to our base-case ACDC_DB, we introduce a
248  parameter $R$:

$$R_X = \frac{\sum_i^n (X_i/\text{ACDC\_DB}_i)}{n}$$

250  where $\text{ACDC\_DB}_i$ and $X_i$ denote the simulated $J_{1.4}$ by the base-case ACDC_DB and
251  another specific parameterization X, respectively, given the input scenarios of $i$ (a set
252  of input values for $T$, CS, concentration of SA ([SA]) and DMA ([DMA])), and $n$
253  signifies the total number of input scenarios.

254

255  **Table 1.** Summary of various cluster dynamics-based parameterizations of SA-DMA
256  nucleation in this study (main parameterizations are in bold, while test ones in regular)

| Case | Description |
| --- | --- |
| **Dynamic_Sim** | Reported parameterization from Li et al. 2023 combining the simplifications in boundary conditions, cluster evaporations, and cluster number |
| **ACDC_DB** | ACDC-derived parameterization coupling DLPNO-CCSD(T)/aug-cc-pVTZ//ωB97X-D/6-311++G(3df,3pd) level of theory, namely the latest theoretical approach |
| ACDC_DB_BC | ACDC-derived parameterization coupling DLPNO-CCSD(T)/aug-cc-pVTZ//ωB97X-D/6-311++G(3df,3pd) level of theory and simplification in boundary conditions (only (SA)₄(DMA)₄ cluster is |

| | |
|---|---|
| | set as boundary condition) |
| ACDC_DB_CE | ACDC-derived parameterization coupling DLPNO-CCSD(T)/aug-cc-pVTZ//ωB97X-D/6-311++G(3df,3pd) level of theory and simplification in cluster evaporations (the evaporation rates of $(SA)_k(DMA)_k$ ($k$ = 2-3) and $(SA)_2(DMA)_1$ clusters are kept zero) |
| ACDC_DB_CN | ACDC-derived parameterization coupling DLPNO-CCSD(T)/aug-cc-pVTZ//ωB97X-D/6-311++G(3df,3pd) level of theory and simplification in cluster number (only $(SA)_k(DMA)_k$ ($k$ = 1-3) and $(SA)_2(DMA)_1$ clusters are involved) |
| **ACDC_RM_SF0.5** | ACDC-derived parameterization coupling RI-CC2/aug-cc-pV(T+d)Z//M06-2X/6-311++G(3df,3pd) level of theory and a SF of 0.5 is applied in collision process, namely the traditional theoretical approach |
| ACDC_RM | ACDC-derived parameterization coupling RI-CC2/aug-cc-pV(T+d)Z//M06-2X/6-311++G(3df,3pd) level of theory and a SF of 1 is applied |

257

**2.2 Incorporating the ACDC-derived Parameterizations into WRF-Chem/R2D-VBS Model**

Various parameterizations are subsequently implemented in the Weather Research and Forecasting-Chemistry model (WRF-Chem) integrating an experimentally constrained Radical Two-Dimensional Volatility Basis Set (2D-VBS) (denoted as WRF-Chem/R2D-VBS) (Zhao et al., 2020). Incorporating the box-model ACDC into a 3-D model using the explicit mathematical formula, as Dynamic_Sim, proves to be challenging. Here, we created a four-dimensional look-up table that delineates the response of $J_{1.4}$ to four input variables ($T$, CS, [SA], and [DMA]) for each ACDC-derived parameterization (Yu, 2010). The table is derived based on multiple ACDC runs by varying input variables. The ranges for the input variables correspond to typical conditions of the atmosphere. Except for $T$, the ranges of variation for all other variables exceed at least one order of magnitude. Therefore, temperature is assumed to follow arithmetic uniform distribution, while the other variables are assumed to follow geometric uniform distribution. Details for the input variables are given in Table S1. In WRF-Chem/R2D-VBS simulations, $J_{1.4}$ are online calculated by interpolating values from a look-up table based on real-time input parameters. In our previous study, we have developed an emission inventory for China and its surrounding regions (Li et al., 2023c). Here [DMA] is calculated in WRF-Chem/R2D-VBS based on a comprehensive source-sink representation of DMA. More details of including DMA in WRF-Chem/R2D-VBS can be found in our previous study (Li et al., 2023c). In addition, a time-integrated-average [DMA] as well as [SA] of each time step were used to drive

280 SA-DMA nucleation, since SA-DMA nucleation is accompanied with condensation of
281 gaseous SA and DMA on pre-existing aerosols simultaneously in the atmosphere.

282 Besides SA-DMA nucleation, seven other nucleation mechanisms have already
283 been incorporated in WRF-Chem/R2D-VBS (Zhao et al., 2020), including neutral/ion-
284 induced SA~~H$_2$SO$_4$~~-H$_2$O nucleation, neutral/ion-induced SA~~H$_2$SO$_4$~~-NH$_3$-H$_2$O
285 nucleation, neutral/ion-induced pure organics nucleation, and SA~~H$_2$SO$_4$~~-organics
286 nucleation. The organics involved in nucleation are ultralow- and extremely low-
287 volatility organic compounds (ULVOC and ELVOC) with O:C >0.4. The formation
288 chemistry of ULVOC and ELVOC from monoterpenes, including autoxidation and
289 dimerization, is traced by the R2D-VBS framework (Zhao et al., 2020). Note that the
290 impact of the other seven mechanisms on particle formation rates and particle number
291 concentration is low compared to SA-DMA as revealed by our previous study (Li et al.,
292 2023c). In WRF-Chem/R2D-VBS, the evolution of PNSDs from 1nm to 10 μm is
293 treated by MOSAIC (Model for Simulating Aerosol Interactions and Chemistry)
294 module. The newly formed 1.4 nm particles from SA-DMA nucleation are injected into
295 the smallest size bin (1 - 1.5 nm) of the MOSAIC.

**2.3 Configurations of WRF-Chem/R2D-VBS Model**

297 The WRF-Chem/R2D-VBS model, incorporating various cluster dynamics-based
298 SA-DMA nucleation parameterizations, was employed in a simulation over a domain
299 with a spatial resolution of 27 km. This domain covers eastern Asia, with Beijing
300 situated close to the center of the simulation area. Details of model configurations can
301 be found in our previous study (Li et al., 2023c). Briefly, we use the ABaCAS-EI 2017
302 and IIASA 2015 emission inventories for mainland China and other areas in the domain,
303 respectively, to represent the anthropogenic emissions (Zheng et al., 2019; Li et al.,
304 2017; Li et al., 2023b); we use Model of Emissions of Gases and Aerosols from Nature
305 (MEGAN) v2.04 to calculate the biogenic emissions (Guenther et al., 2006). To
306 accurately represent the variation and distribution of chemical species concentrations
307 during the simulation period, the chemical initial conditions, which represent the
308 concentration field of chemical species at the initial simulation time, and the boundary
309 conditions, which represent the flux or concentration around the simulation domain
310 during the simulation period (Brasseur et al., 2017), are used in our WRF-Chem/R2D-
311 VBS simulations. The simulation results from the National Center for Atmospheric
312 Research's Community Atmosphere Model with Chemistry
313 (https://www.acom.ucar.edu/cam-chem/cam-chem.shtml) is used for the chemical
314 initial and boundary conditions in WRF-Chem/R2D-VBS simulations. In addition, we
315 use a 5-day spin-up to minimize the impact of chemical initial conditions on simulation
316 results.

317 The simulation period consists of two parts: the winter period, which spans from
318 January 14 to January 31, 2019, and the summer period, which is from August 18 to
319 August 31, 2019. Previous observational studies have shown that the particle formation
320 rates reach their highest and lowest levels during winter and summer in China,
321 respectively (Deng et al., 2020; Chu et al., 2019). Therefore, periods from these two

Formatted: Font color: Auto

322  seasons are selected as representative simulation periods in this study and the specific
323  time periods corresponded to those with relatively complete and continuous PNSDs and
324  $J_{1.4}$ observations. Since observational data for DMA concentration is only available for
325  the period from January 1, 2019 to January 23, 2019, similar to our other study (Ning
326  et al., 2024), we performed additional simulation for this period to compare
327  observational and simulated DMA concentrations. For each season, all the SA-DMA
328  parameterizations listed in Table 1 were employed for simulation. Among them,
329  ACDC_DB, Dynamic_Sim, and ACDC_RM_SF0.5 serve as three main
330  parameterizations, while ACDC_DB_CE, ACDC_DB_BC, ACDC_DB_CN, and
331  ACDC_RM are set as test cases to investigate the impact of individual simplification
332  or theoretical approach on NPF simulations. In all comparisons, ACDC_DB is set as a
333  reference.

334  **2.4 Ambient Measurements**

335  In the 3-D simulations, we utilize measured concentrations of nucleation precursors
336  and PNSDs as a criterion to discuss the model performance with various
337  parameterizations. The duration of the observational data matches that of the
338  simulations mentioned above. Detailed descriptions of the observation site and
339  instruments can be found in our previous research (Deng et al., 2020; Zhu et al., 2022).
340  Briefly, the observation site is located on the West Campus of the Beijing University of
341  Chemical Technology. CI-TOF-MS (chemical ionization time-of-flight mass
342  spectrometer; Aerodyne Research Inc.) were used to measure the concentrations of SA.
343  Amine concentrations were measured with a modified TOF-MS using $H_3O^+$ or its
344  clusters as the reagent ions (Zhu et al., 2022). PNSDs from 1 nm to 10 µm were
345  measured using a PSD (particle size distribution) system and a DEG-SMPS (diethyl
346  glycol scanning mobility particle spectrometer). $J_{1.4}$ derived from observation is
347  calculated employing an improved aerosol population balance formula (Cai and Jiang,
348  2017).

349

350 **3 RESULTS AND DISCUSSIONS**
351 **3.1 Comparison of Different Parameterizations Based on Box-Model Simulations**
352 **3.1.1 Comparison between ACDC_DB and Dynamic_Sim**
353    Figure 1 illustrates the comparison between the reported cluster dynamics-based
354 parameterization with simplifications, Dynamic_Sim, and the base-case
355 parameterization ACDC_DB. The comparison is based on a comprehensive dataset that
356 includes over 40,000 box-model simulations for each parameterization, by varying
357 parameters such as [SA] ($1 \times 10^5 - 1 \times 10^8$ molec. cm$^{-3}$), [DMA] ($5 \times 10^6 - \underline{5\bcancel{1}} \times 10^8$
358 molec. cm$^{-3}$), CS ($5 \times 10^{-4} - 5 \times 10^{-1}$ s$^{-1}$), and $T$ (250 – 320 K). In most scenarios, $J_{1.4}$
359 predicted by ACDC_DB and Dynamic_Sim demonstrates deviations within one order
360 of magnitude, with the majority falling within a factor of 3. However, Dynamic_Sim
361 predicts notably higher $J_{1.4}$ than ACDC_DB in scenarios where $T$ exceeds ~300 K and
362 CS is below ~$3 \times 10^{-3}$ s$^{-1}$, characteristic of a clean atmosphere during summer. The
363 discrepancy in these scenarios elevates the overall $R_{\text{Dynamic\_Sim}}$ up to 17.0. Furthermore,
364 no clear correlation is observed between the differences of the two parameterizations
365 and other input parameters such as [DMA] and [SA] (Figure S2). The differences
366 between parameterizations are attributed to the combined effects of the three
367 simplifications and the lower $\Delta G$ of (SA)$_1$(DMA)$_1$ cluster in Dynamic_Sim. However,
368 the latter should not be the primary cause for the significant differences of $J_{1.4}$ prediction
369 under high $T$ and low CS conditions, as it typically results in an overestimation within
370 an order of magnitude ($R$=3.3) (Figure S1).
371
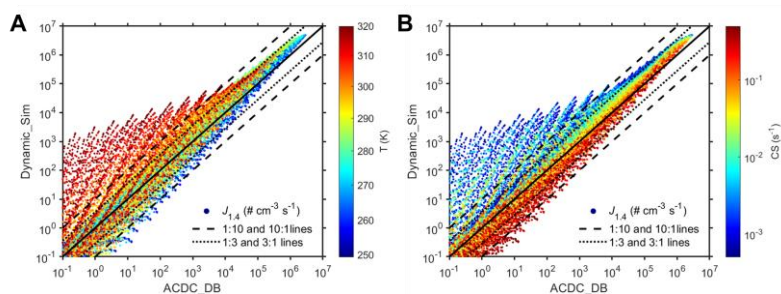
373 **Figure 1.** Comparison of $J_{1.4}$ predictions between ACDC_DB and Dynamic_Sim
374 correlated with $T$ variation (A) and CS variation (B). Solid dots represent simulated $J_{1.4}$
375 values, solid lines indicate a 1:1 line, dotted lines correspond to 1:3 and 3:1 lines, and
376 dashed lines represent 1:10 and 10:1 lines.
377

378    The impacts of the three simplifications made in Dynamic_Sim are shown in Figure
379 2. Specifically, the simplification in cluster evaporations tends to elevate the predicted
380 $J_{1.4}$, whereas the simplifications in boundary conditions and cluster number tend to
381 lower them. When applying the simplification in cluster evaporations (clusters larger
382 than (SA)$_1$(DMA)$_1$ are regarded stable with no evaporation) to ACDC_DB, the
383 predicted $J_{1.4}$ by ACDC_DB_CE only slightly exceed than that of ACDC_DB within a

384  factor of 3 under conditions where $T <$ ~290 K and CS > ~0.1 s$^{-1}$. However, the
385  overestimation of $J_{1.4}$ prediction by ACDC_DB_CE becomes much greater with
386  increasing $T$ and decreasing CS. The discrepancy between ACDC_DB_CE and
387  ACDC_DB should be primarily attributed to the pivotal role of $T$ in influencing cluster
388  evaporation rates (Ortega et al., 2012; Deng et al., 2020). At low $T$, the evaporation
389  rates of clusters are low enough to allow efficient nucleation, thus whether setting the
390  concerned SA-DMA clusters to evaporate based on the expected evaporation rates does
391  not lead to a significant impact on $J_{1.4}$ prediction. However, at high $T$, the evaporation
392  rates of clusters significantly increase, therefore the simplification in cluster
393  evaporations within ACDC_DB_CE is likely to predict higher $J_{1.4}$ than those with no
394  simplification. The impact of simplification in cluster evaporations across varying $T$ is
395  also found in a nonbranched SA-DMA nucleation scheme from 280 K to 298 K reported
396  by Li et al. (2023a). Note also that the overestimation of ACDC_DB_CE diminishes as
397  CS increases (Figure 2D), with CS becoming the primary sink in the nucleation system
398  and the impact of cluster evaporations becoming less pronounced. This underscores the
399  connection between the specific deviation arising from simplification in cluster
400  evaporations and the respective contributions of CS and cluster evaporations to the
401  overall sink for clusters in nucleation. In addition, the relative independence of the
402  differences between ACDC_DB_CE and ACDC_DB from variations in precursor
403  concentrations ([SA] and [DMA]) is similar to that between Dynamic_Sim and
404  ACDC_DB (Figure S3). Overall, the scenarios where ACDC_DB_CE predicts higher
405  $J_{1.4}$ than ACDC_DB only occurs under conditions of both high $T$ and low CS (Figure
406  2A and Figure 2D). The averaged discrepancy between ACDC_DB_CE and
407  ACDC_DB $R_{ACDC\_DB\_CE}$ is 22.3, closely resembling $R_{Dynamic\_Sim}$, indicating that the
408  simplification in cluster evaporations is a major factor contributing to the difference
409  between Dynamic_Sim and ACDC_DB.
410
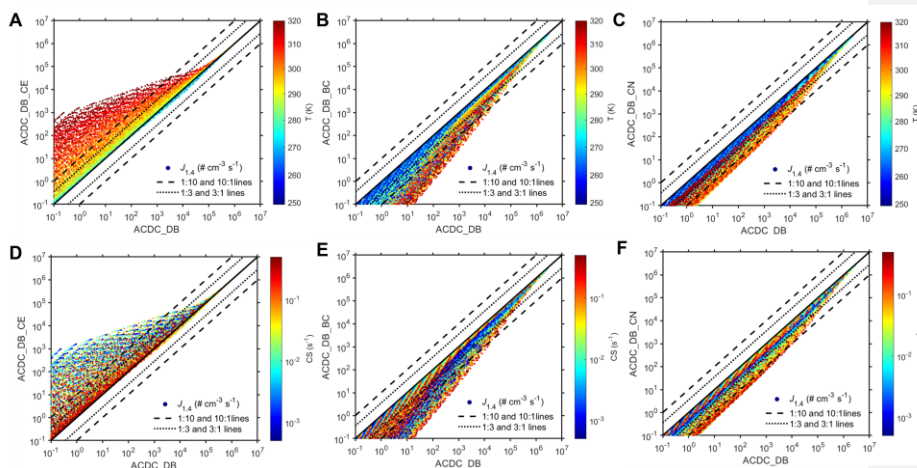
412  **Figure 2.** Comparison of $J_{1.4}$ predictions between ACDC_DB and test cases including

413    ACDC_DB_CE (A and D), ACDC_DB_BC (B and E), and ACDC_DB_CN (C and F).

414    The first row in the panel (A, B and C) is correlated with $T$ variation and the second

415    row (D, E and F) is correlated with CS variation. Solid dots represent simulated $J_{1.4}$

416    values, solid lines indicate a 1:1 line, dotted lines correspond to 1:3 and 3:1 lines, and

417    dashed lines represent 1:10 and 10:1 lines.

418

419        The underestimations of ACDC_DB_BC and ACDC_DB_CN in $J_{1.4}$ prediction

420    compared to base-case ACDC_DB are related to the growth pathways of SA-DMA

421    clusters. In the original scheme of ACDC_DB, precursor molecules have the flexibility

422    to pass through any $(SA)_m(DMA)_n$ clusters ($0 < n \leqslant m \leqslant 3$), and terminal 1.4-nm

423    particles are formed when the clusters grow to $(SA)_4(DMA)_4$ or $(SA)_4(DMA)_3$. As

424    expected, ACDC_DB_BC, which assumes $(SA)_4(DMA)_4$ cluster as the only boundary

425    condition with an omission of $(SA)_4(DMA)_3$ cluster, predicts lower $J_{1.4}$ than ACDC_DB.

426    $(SA)_4(DMA)_3$ and $(SA)_4(DMA)_4$ clusters are primarily formed from $(SA)_3(DMA)_3$

427    cluster by colliding with a SA molecule and a $(SA)_1(DMA)_1$ cluster, respectively. As

428    the concentration of $(SA)_1(DMA)_1$ cluster is more sensitive to $T$, we further found that

429    the discrepancy between ACDC_DB_BC and ACDC_DB becomes more pronounced

430    with increasing $T$ (Figure 2B). Furthermore, we found no apparent correlation between

431    the variation of CS and the disparity between ACDC_DB_BC and ACDC_DB (Figure

432    2E).

433        In addition to ACDC_DB_BC, ACDC_DB_CN also underestimates $J_{1.4}$ compared

434    to ACDC_DB with a comparable value ($\sim$0.5) of $R_{ACDC\_DB\_CN}$ and $R_{ACDC\_DB\_BC}$. Under

435    the simplification in cluster number, the formation of 1.4-nm clusters can only occur

436    through specific pathways, including $(SA)_1(DMA)_1 \rightarrow (SA)_2(DMA)_2 \rightarrow (SA)_3(DMA)_3$

437    $\rightarrow (SA)_4(DMA)_4/(SA)_4(DMA)_3$, $(SA)_1(DMA)_1 \rightarrow (SA)_2(DMA)_1 \rightarrow (SA)_2(DMA)_2 \rightarrow$

438    $(SA)_3(DMA)_3 \rightarrow (SA)_4(DMA)_4/(SA)_4(DMA)_3$, or a combination thereof, while other

439    pathways are restricted. Due to the variability in growth pathways and their

440    contributions to $J_{1.4}$ under different atmospheric conditions, the difference between

441    ACDC_DB_CN and ACDC_DB is not strongly correlated with the variations of $T$ and

442    CS (Figure 2C and Figure 2F). Despite that, while the differences between the two

443    tested parameterizations (ACDC_DB_BC and ACDC_DB_CN) involving cluster

444    growth pathways and the original ACDC_DB are not highly correlated with [DMA],

445    there is a more pronounced correlation with [SA], which implies a more important role

446    of SA in cluster growth (Figure S4 and Figure S5).

447        In our previous study, we demonstrated improvements in computing CS- dependent

448    $J_{1.4}$ of SA-DMA nucleation with the Dynamic_Sim compared to the previous power-

449    law parameterizations under polluted atmospheric conditions (Li et al., 2023c). Here,

450    we further show that, based on Dynamic_Sim, the new ACDC_DB with complete

451    cluster dynamics can more reasonably simulate $J_{1.4}$ under previously less studied

452    conditions of high $T$ ($> \sim$300 K) and low CS ($< \sim 3 \times 10^{-3}$ s$^{-1}$), where Dynamic_Sim tends

453    to produce significant overestimation of $J_{1.4}$. This overestimation is primarily driven by

454    the simplification in cluster evaporations within Dynamic_Sim. Even though a

455    comparable performance in $J_{1.4}$ prediction between ACDC_DB and Dynamic_Sim
456    could be achieved under other ambient conditions, cautions should be made that the
457    mutual offsetting effect between overestimation and underestimation resulting from
458    different simplifications in Dynamic_Sim when computing $J_{1.4}$.
459    **3.1.2 Comparison between ACDC_DB and ACDC_RM_SF0.5**
460        In Figure 3, ACDC_DB is compared with another main ACDC-derived
461    parameterization, ACDC_RM_SF0.5, which uses the RI-CC2/aug-cc-pV(T+d)Z//M06-
462    2X/6-311++G(3df,3pd) level of theory and employs a SF of 0.5 in processing collision.
463    It can be observed that at lower temperatures (~280 K), ACDC_RM_SF0.5 and
464    ACDC_DB exhibit similar performance in predicting $J_{1.4}$. However, with higher $T$
465    (accompanied by lower CS with a slight dependency), $J_{1.4}$ predicted by
466    ACDC_RM_SF0.5 become higher than that predicted by ACDC_DB, reaching even
467    several orders of magnitude at the upper limit of the $T$ range (320 K). Furthermore, we
468    also observed that in scenarios close to the lower limit of the $T$ range (250 K), the $J_{1.4}$
469    predicted by ACDC_RM_SF0.5 shift from being higher to lower compared to
470    ACDC_DB.
471
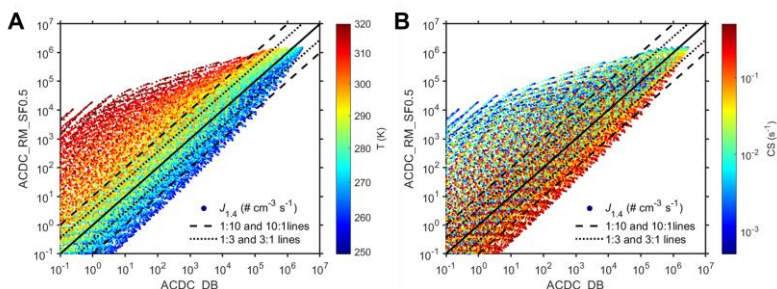
472
473    **Figure 3.** Comparison of $J_{1.4}$ predictions between ACDC_DB and ACDC_RM_SF0.5
474    correlated with $T$ variation (A) and CS variation (B). Solid dots represent simulated $J_{1.4}$
475    values, solid lines indicate a 1:1 line, dotted lines correspond to 1:3 and 3:1 lines, and
476    dashed lines represent 1:10 and 10:1 lines.
477
478        The distinction between ACDC_RM_SF0.5 and ACDC_DB arises from the
479    combined effects of variation in quantum chemical calculation method and the
480    application of the 0.5 SF in collision processing. As depicted in Figure 4, when the SF
481    in ACDC_RM_SF0.5 is set to unity as in ACDC_DB, the resulting ACDC_RM
482    parameterization predicts consistently higher $J_{1.4}$ than ACDC_DB. This implies that the
483    modified quantum chemical calculation method, which results in lower evaporation
484    rates for clusters within the system compared to ACDC_DB under the same condition,
485    leads to higher $J_{1.4}$ predictions. The impact from varying quantum chemical calculation
486    method is akin to that from simplification in cluster evaporations discussed earlier. The
487    distinction between ACDC_RM and ACDC_DB_CE lies in the fact that the modified
488    quantum chemical calculation method affects all clusters within the system, whereas

489    the simplification in cluster evaporations is specific to limited clusters. This contributes

490    to a much higher $R_{ACDC\_RM}$ (614.5) compared to $R_{ACDC\_DB\_CE}$ (22.3). Despite that,

491    compared to ACDC_DB, the differences for both ACDC_DB_CE, ACDC_RM, as well

492    as ACDC_RM_SF0.5 demonstrate similar sensitivity to $T$ (Figure 3A and Figure 4A)

493    and CS (Figure 3B and Figure 4B) but independence on [SA] (Figure S6A and Figure

494    S7A) and [DMA] (Figure S6B and Figure S7B). Comparing ACDC_RM_SF0.5 and

495    ACDC_RM, it can be inferred that the application of a 0.5 SF in collision processes

496    would result in an underestimation in $J_{1.4}$ prediction. It can be noted that in most

497    previous studies (Almeida et al., 2013; Kürten et al., 2018; Elm et al., 2020),

498    comparisons of ACDC simulations using the traditional method and measured particle

499    formation rates are conducted at around 280 K. At this temperature, all three main

500    parameterizations of ACDC_RM_SF0.5, ACDC_DB, and Dynamic_Sim tends to yield

501    similar $J_{1.4}$ predictions and should have consistent applicability in NPF simulation.

502
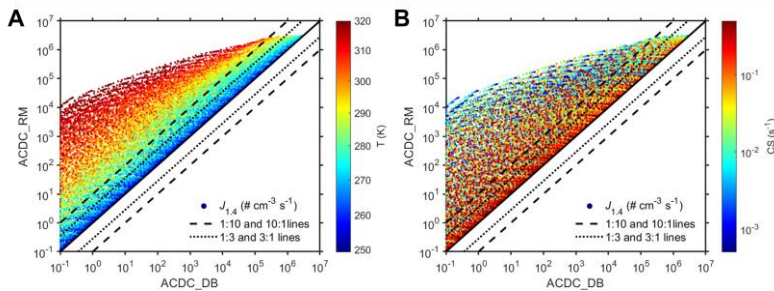
504    **Figure 4.** Comparison of $J_{1.4}$ predictions between ACDC_DB and ACDC_RM

505    correlated with $T$ variation (A) and CS variation (B). Solid dots represent simulated $J_{1.4}$

506    values, solid lines indicate a 1:1 line, dotted lines correspond to 1:3 and 3:1 lines, and

507    dashed lines represent 1:10 and 10:1 lines.

508

509    In summary, based on our base-case parameterization ACDC_DB, the extensive

510    box model simulations above demonstrate the characteristics and applicability

511    conditions of different parameterizations. Specifically, Dynamic_Sim shows general

512    consistency with ACDC_DB in simulating $J_{1.4}$is applicable under most atmospheric

513    conditions with $T <$ ~300 K orand CS > ~3.0×10⁻³ s⁻¹, while overestimating $J_{1.4}$ with $T >$

514    ~300 K and CS > ~3.0×10⁻³ s⁻¹ compared to ACDC_DB. ACDC_RM_SF0.5 performs

515    similarly to ACDC_DBis suitable under conditions of ~with $T$ around 280 K but give

516    different $J_{1.4}$ predictions at other temperatures. We further use reported measurements

517    from well-controlled CLOUD chamber experiments to examine the characteristics and

518    applicability of these parameterizations (Xiao et al., 2021). As shown in Figure S8,

519    simulated $J_{1.4}$simulations using three main parameterizations, ACDC_DB,

520    ACDC_RM_SF0.5, and Dynamic_Sim, correspond well to measured $J_{1.7}$experimental

521    results at low temperature ($T$ = 278 K), proving the applicability of all three

522    parameterizations at this temperature. In the experiments with elevated temperature ($T$

523 = 293 K), ACDC_DB and Dynamic_Sim continues to exhibit similar performance, with
524 slight overestimation by approximately 2 factors. This may be because the much lower
525 cluster concentrations at high temperatures compared to those at low temperatures lead
526 to slower cluster growth and thus an enlarged gap between $J_{1.4}$ and $J_{1.7}$ (Figure
527 S9).~~simulated results still corresponding to experimental results.~~ In contrast,
528 ACDC_RM_SF0.5 only shows a slight $T$-dependence, which is deviated from the
529 measurements. The comparison between controlled experiments and box-model
530 simulations hence confirms our conclusions above, and provides a solid basis for further
531 discussions on 3-D simulations using these parameterizations with constraint from field
532 observations.

**3.2 Comparison of Different Parameterizations Based on 3-D Model Simulations**

534 Various cluster dynamics-based parameterizations for SA-DMA nucleation were
535 subsequently integrated into the WRF-Chem/R2D-VBS model. 3-D simulations using
536 these parameterizations have been conducted for both wintertime and summertime
537 conditions in Beijing. Given that the concentrations of precursors are crucial input
538 variables for each parameterization, the simulated and observed concentrations of
539 [DMA] and [SA] are compared. Figure S10~~S9~~, Figure S11~~0~~ and Table S2 illustrates
540 good consistencies in temporal variations and the mean values between simulations and
541 observations in Beijing. This validates the reliability of our representation of sources
542 and sinks for nucleating precursors and serves as a foundation for our discussions on
543 the performances of various parameterizations. In the following sections, we discuss
544 the results of 3-D NPF simulations in Beijing during winter and summer by employing
545 different parameterizations. The evaluation of various parameterizations focuses on
546 their ability to reproduce in situ NPF measurements across different seasons.

**3.2.1 Wintertime Simulations**

548 Figure 5A and Figure S12~~1~~A primarily compare the simulated $J_{1.4}$ values from
549 different parameterizations with those derived from wintertime observations in Beijing,
550 as $J_{1.4}$ being a key parameter describing NPF events. The performance of Dynamic_Sim
551 in simulating $J_{1.4}$ during wintertime Beijing has been discussed in our previous study
552 (Li et al., 2023c). The averaged $J_{1.4}$ simulated by three main parameterizations
553 (Dynamic_Sim: 64.0 cm$^{-3}$ s$^{-1}$; ACDC_DB: 51.6 cm$^{-3}$ s$^{-1}$; ACDC_RM_SF0.5: 54.5 cm$^{-3}$
554 $^{3}$ s$^{-1}$) approximate the observation (46.7 cm$^{-3}$ s$^{-1}$). For test cases, however, only
555 ACDC_DB_CE (55.7 cm$^{-3}$ s$^{-1}$) demonstrates a reasonable representation of $J_{1.4}$. $J_{1.4}$
556 simulated from ACDC_DB_BC (20.5 cm$^{-3}$ s$^{-1}$) and ACDC_DB_CN (20.8 cm$^{-3}$ s$^{-1}$) are
557 approximately two times lower than the observed values, while ACDC_RM (226.2 cm$^{-3}$
558 $^{3}$ s$^{-1}$) is approximately five times higher than the observations.

559 The performances of different parameterizations on depicting $J_{1.4}$ subsequently
560 influences their representations of PNSDs evolution and NPF events, which are shown
561 in Figure 5B. Generally, most parameterizations efficiently reproduce the observed time
562 evolution of PNSDs and captures NPF events, such as those on 01/20, 01/21, 01/30,
563 and 01/31, which are characterized by the burst of aerosol number concentrations in
564 nanometer-sized range. Simulations using ACDC_DB_BC and ACDC_DB_CN result

Formatted: Font color: Auto

565  in lower particle concentrations in the low size range (1-10 nm) during the NPF period
566  compared to three main parameterizations and the observations, while simulations with
567  ACDC_RM show higher concentrations. This is consistent with the comparison of $J_{1.4}$
568  among different parameterizations and further evident by the comparison of averaged
569  PNSDs in Figure 5C. Notably, when compared to observations, all parameterizations
570  consistently underestimate the averaged PNSDs within the 2-10 nm range but
571  overestimate them in the 10-50 nm range. This discrepancy may stem from simplified
572  assumptions in particle growth simulation, as discussed in our previous study (Li et al.,
573  2023c).

574
575
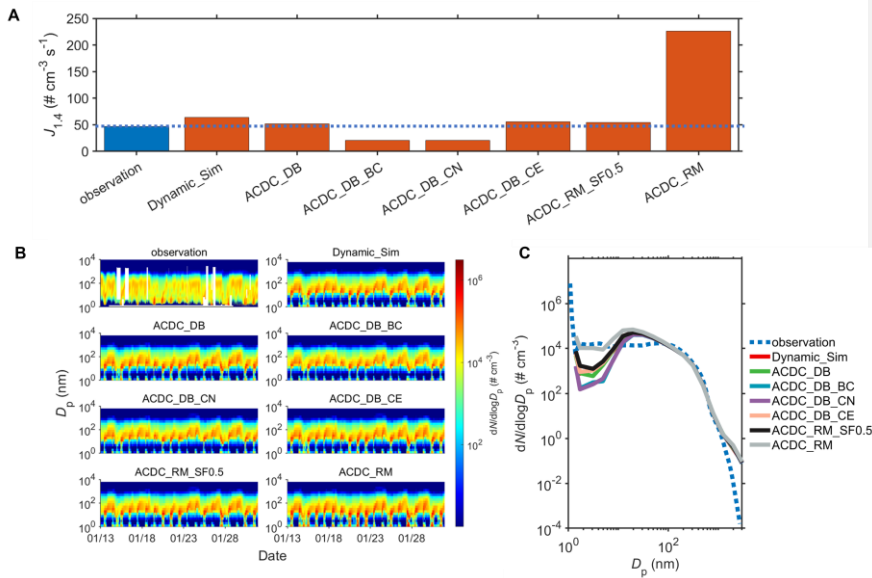
576
577  **Figure 5.** Comparison of simulated particle formation rates and particle number size
578  distributions (PNSDs) with observations during January 13, 2019, to January 31, 2019,
579  in Beijing. A represents the averaged particle formation rates during the period, the blue
580  bars and orange bars represent observations and simulations, respectively, while the
581  blue dashed line represents the observed values. Daily maximum values of $J_{1.4}$ are used
582  following Deng et al. (2020); B for the time series of PNSDs; and C for the averaged
583  PNSDs.

584
585      The results show the applicability of all three main parameterizations in NPF
586  modeling during wintertime periods. Importantly, the reliability of the new ACDC-
587  derived parameterization based on the latest theoretical approach (ACDC_DB) without
588  simplifications in 3-D NPF simulation, is affirmed. The differences among various
589  parameterizations can be explained by the comprehensive box-model simulations

590     above at corresponding conditions. Compared to ACDC_DB, the $J_{1.4}$ and PNSDs
591     simulated by other two main parameterizations (Dynamic_Sim and ACDC_RM_SF0.5)
592     agree similarly with observations, but for different reasons. In the case of Dynamic_Sim,
593     the simplification in cluster evaporations has minimal impact on NPF simulation since
594     CS is the dominant sink for clusters under the wintertime conditions (averaged $T$ and
595     CS is 274.7 K and $3.3 \times 10^{-2}$ s$^{-1}$, respectively). However, the simplifications in boundary
596     conditions and cluster number lead to the underestimation of the $J_{1.4}$, consequently
597     lowering the simulated particle number concentrations in 1-100 nm size range due to
598     the ignorance of clusters contributing to growth. As a result, the agreement of
599     Dynamic_sim to observations should result from a combination of underestimation due
600     to simplifications in boundary conditions and cluster number, along with the
601     compensatory effect of the overestimation caused by lower $\Delta G$ for $(SA)_1(DMA)_1$
602     cluster. For another main parameterization ACDC_RM_SF0.5, since the test
603     parameterization ACDC_RM considerably overestimates $J_{1.4}$ and PNSDs compared to
604     the observations, the general agreement between ACDC_RM_SF0.5 and observations
605     should be attributed to a balance between reduced kinetic limit through the application
606     of SF and the compensatory effect of the overestimation caused by inappropriate
607     representation of cluster thermodynamics.

608 **3.2.2 Summertime Simulations**

609     Figure 6 provides additional insight into the performance of various
610     parameterizations in NPF simulation during summer. It can be noted that there exists a
611     significant difference in particle formation rates between winter and summer in Beijing.
612     As shown in Figure 6 and Figure S12B, ACDC_DB and Dynamic_Sim continues to
613     demonstrate consistent and effective performance in simulating $J_{1.4}$ (within a factor of
614     2), PNSDs evolution as well as NPF events. However, distinct differences emerge in
615     the NPF simulation for other parameterizations, including another main
616     parameterization ACDC_RM_SF0.5. Specifically, in contrast to the good performance
617     of ACDC_DB and Dynamic_Sim, ACDC_RM_SF0.5, along with the test case
618     ACDC_RM, exhibits a significant overestimation of $J_{1.4}$, exceeding the observations by
619     more than 15 times and over two orders of magnitude, respectively. This aligns with
620     their overestimation of NPF occurrences and particle number concentration in the size
621     range of 1-100 nm in comparison to observation, with a more pronounced
622     overestimation for ACDC_RM. Conversely, the test cases of ACDC_DB_BC and
623     ACDC_DB_CN show an underestimation of averaged $J_{1.4}$ by approximately 4-5 times.
624     They almost fail to depict NPF events, resulting in a significant underestimation of
625     number concentrations in the 1-100 nm size range. Simulations using ACDC_DB_CE
626     notably overestimates $J_{1.4}$ especially on 08/28 – 08/31 (Figure S11B), which results in
627     an overestimation of averaged $J_{1.4}$ by approximately 4 times compared to the
628     observations. However, apart from a moderate overestimation in the initial particle size,
629     we can observe a closer alignment of particle number concentrations in the 2-50 nm
630     range with observations for ACDC_DB_CE, which should result from a combination
631     of surplus newly formed particles and fast particle growth from inadequate assumptions

Formatted: Font color: Auto

632 within the model. For the broader 2-100 nm size range, it can be observed that
633 ACDC_DB and Dynamic_Sim are closer to the observations compared to
634 ACDC_DB_CE and another major parameterization ACDC_RM_SF0.5 (Figure S13).
635 The latter two overestimate the average number concentrations during the simulation
636 period by 1.6 times and 2.5 times, respectively. Given the more accurate representation
637 of nucleation rates by ACDC_DB and Dynamic_Sim, the discrepancies in the 2-100
638 nm size range compared to the observed PNSDs should also stem from the simplified
639 assumptions in particle growth simulations.
640
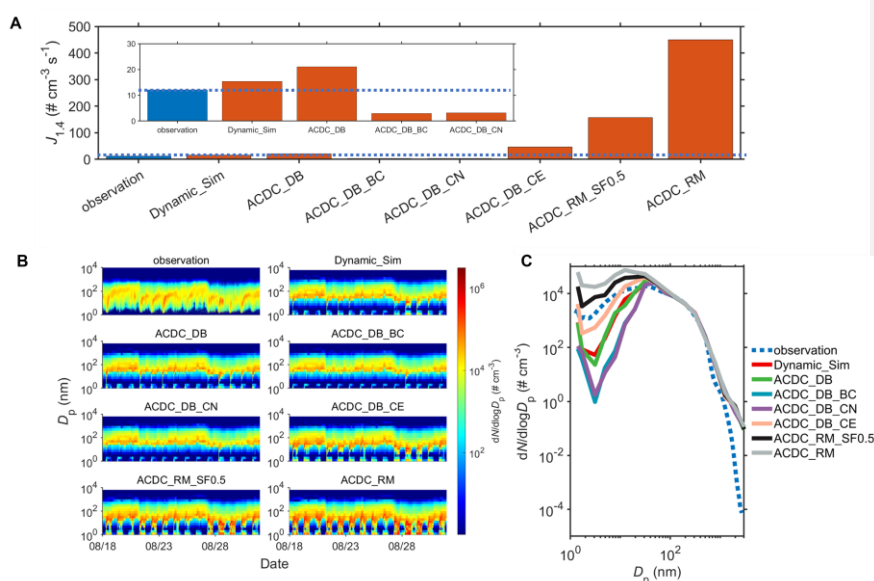
641

642 **Figure 6.** Comparison of simulated particle formation rates and particle number size
643 distributions (PNSDs) with observations during August 18, 2019, to August 31, 2019,
644 in Beijing. A represents the averaged particle formation rates during the period, the blue
645 bars and orange bars represent observations and simulations, respectively, while the
646 blue dashed line represents the observed values. Daily maximum values of $J_{1.4}$ are used
647 following Deng et al. (2020); B for the time series of PNSDs; and C for the averaged
648 PNSDs.

649

650     Most previous NPF studies combining experiments/observations with simulations
651 are conducted under conditions biased towards winter (~280K) (Almeida et al., 2013;
652 Lu et al., 2020). Under summer conditions with elevated $T$, there exists a deficiency in
653 parameterization evaluations for simulating NPF. The 3-D simulation results during the
654 summer period provide additional validation for the reliability of ACDC_DB. For
655 ACDC_RM_SF0.5, evidence from both box-model simulations and 3-D simulations
656 suggests that it can accurately reproduce real SA-DMA nucleation at temperatures

657 around 280 K, while it has limitations in higher temperatures. Another main
658 parameterization Dynamic_Sim consistently demonstrates good performance in NPF
659 simulation, akin to its efficacy in winter conditions. With the increased temperature in
660 summer (averaged $T$ is 298.2 K), the influence of simplifications in cluster evaporations,
661 cluster number, and boundary conditions becomes more profound, mirroring the trends
662 observed in box-model simulations above. This leads to more significant
663 overestimation for ACDC_DB_CE, and underestimation for ACDC_DB_CN and
664 ACDC_DB_BC compared to the observation as well as the base-case ACDC_DB. Note
665 that CS during the summer period (averaged CS is $2.8\times10^{-2}$ s$^{-1}$) decreases compared to
666 winter but remains significantly higher than typical values in clean regions ($\sim3.0\times10^{-3}$
667 s$^{-1}$) (Dal Maso et al., 2008). According to the limited conditions for Dynamic_Sim
668 described above, although the overestimation of $J_{1.4}$ prediction resulting from the
669 simplification in cluster evaporations is more pronounced in summer compared to that
670 in winter, impacts from diverse overestimations and underestimations from different
671 simplifications and varied thermodynamics for $(SA)_1(DMA)_1$ cluster can still offset
672 each other, thereby allowing Dynamic_Sim to match observations. Based on previous
673 comparisons using box-models, significant differences in $J_{1.4}$ predictions between
674 Dynamic_Sim and ACDC_DB only exist under conditions of high $T > \sim300$ K and low
675 CS $< \sim3\times10^{-3}$ s$^{-1}$, thus similar performance of Dynamic_Sim and ACDC_DB can be
676 expected in the polluted atmosphere (CS $> \sim1.0\times10^{-2}$ s$^{-1}$). In clean atmosphere with
677 high temperature, however, caution is advised when using Dynamic_Sim for 3-D NPF
678 simulations.

679 **4. CONCLUSIONS and DISCUSSIONS**

680 By integrating box modeling, 3-D simulations, also under the constraint from in
681 situ measurements, this study conducts comprehensive comparison of different cluster
682 dynamics-based parameterizations for SA-DMA nucleation. Among them, the ACDC-
683 derived parameterization grounded in the latest molecular-level understanding and
684 complete representation of cluster dynamics (ACDC_DB), is identified to effectively
685 model particle formation rates and PNSDs evolution in both winter and summer in
686 Beijing within 3-D simulations. While a previously proposed simplified cluster
687 dynamics-based parameterization (Dynamic_Sim) performs comparably in modeling
688 NPF in Beijing, analysis reveals that their similarity arises from a delicate balance
689 between overestimation and underestimation due to simplifications in cluster dynamics
690 processes and the difference in thermodynamics of initial cluster. Particularly, under
691 specific conditions of high temperature ($> \sim300$ K) and low CS ($< \sim3\times10^{-3}$ s$^{-1}$),
692 Dynamic_Sim tends to make significant overestimation of particle formation rates
693 compared to the reality. Moreover, the study furnishes evidence that integrating ACDC-
694 derived parameterizations with the traditional theoretical approach RI-CC2/aug-cc-
695 pV(T+d)Z//M06-2X/6-311++G(3df,3pd) (ACDC_RM_SF0.5) effectively captures
696 particle formation rates and the evolution of PNSDs around 280 K, a temperature range
697 frequently explored in prior experiments and simulations investigating NPF (Kirkby et
698 al., 2011; Almeida et al., 2013; Kirkby et al., 2016; Xie et al., 2017; He et al., 2021; Ma

699 et al., 2019). Therefore, ACDC_RM_SF0.5 exhibits consistent applicability as other
700 two parameterizations at around ~280 K. However, attributed to an inappropriate
701 representation of cluster thermodynamics, ACDC_RM_SF0.5 has limitations in
702 predicting particle formation rates at elevated temperatures. Overall, considering all
703 aspects, we recommend ACDC_DB as a more reliable parameterization for simulating
704 NPF across various atmospheric environments.

705 In addition to contributing to a more reasonable 3-D modeling of NPF, our research
706 further provides valuable references for the development of parameterizations for other
707 nucleation systems. Firstly, we demonstrate the efficacy of the DLPNO-CCSD(T)/aug-
708 cc-pVTZ//ωB97X-D/6-311++G(3df,3pd) level of theory in describing the
709 thermodynamic properties of SA-DMA clusters through comprehensive evidence. This
710 approach can thus be referenced when using quantum chemical calculations to obtain
711 thermodynamic data for other nucleation clusters, especially for other alkylamines such
712 as methylamine/trimethylamine-sulfuric acid clusters. Although DLPNO method still
713 has uncertainties in accurately describing cluster thermodynamics (Besel et al., 2020),
714 it is well recognized as the best available method currently (Elm et al., 2020). Besides,It
715 should be also noted, however, that in some qualitative studies, e.g., comparing the
716 enhancing potential or synergistic effects of different precursors in SA-driven
717 nucleation, methods other than DLPNO-CCSD(T)/aug-cc-pVTZ//ωB97X-D/6-
718 311++G(3df,3pd), such as RI-CC2/aug-cc-pV(T+d)Z//M06-2X/6-311++G(3df,3pd),
719 are equally valid (Liu et al., 2019).

720 ComprehensiveSecondly, we provide comprehensive modeling evidences are
721 provided in this study that certain simplifications or assumptions in cluster dynamics,
722 such as reducing the number of expected clusters, modifying boundary conditions, and
723 assuming certain clusters to be non-evaporative, can significantly impact the prediction
724 of particle formation rates and hence alter the 3-D NPF simulation under certain
725 conditions. While applying certain simplifications concurrently under specific ambient
726 conditions can offset different influences against each other, leading to a satisfactory
727 model-observation comparison, there is a risk that certain simplifications may drive the
728 model''s outcomes away from reality when environmental conditions change.
729 Therefore, caution should be exercised when applying these simplifications in
730 derivation of nucleation parameterizations and subsequent application in 3-D models.
731 In addition to the simplifications within the cluster dynamics regime, it should be noted
732 that current standard treatments in 3-D models that ignore detailed gas-cluster-aerosol
733 interactions may also lead to biases under certain atmospheric conditions (Olenius and
734 Roldin, 2022). This applies not only to parameterizations involving explicit
735 mathematical expressions but also to those using ACDC-derived look-up tables.
736 Additional evaluations for the SA-DMA system indicate that the impacts of these
737 treatments may be highest under a combination of low temperature (< ~270 K), low CS
738 (< ~0.003 s$^{-1}$), and low precursor concentrations, which leads to elevated time to reach
739 steady state and a higher proportion of precursor consumption from cluster formation,
740 as also indicated by Olenius and Roldin's study (Olenius and Roldin, 2022). Despite

741 these impacts being generally limited under most atmospheric conditions in our
742 modeling scenarios (see supporting information), further research, especially using
743 computationally lightweight models, should aim to circumvent the potential bias by
744 linking the cluster and aerosol dynamics (Olenius and Roldin, 2022).
745     It is recognizedLastly, we note that the development of cluster dynamics-based
746 nucleation parameterizations in the form of explicit mathematical expressions is subject
747 to limitations, especially for systems involving multiple precursor species (Semeniuk
748 and Dastoor, 2018). Given that the original ACDC has been extended to involve more
749 than two precursor species, the ACDC-derived parameterization framework, in the form
750 of a look-up table, is highly meaningful for establishing parameterizations for these
751 multi-component nucleation systems. Given that multiple nucleation pathways may be
752 simultaneously considered and simulated in 3-D modeling through ACDC-derived
753 look-up tables, automized incorporation of tables are needed through useful tools such
754 as J-GAIN developed recently (Yazgi and Olenius, 2023).
755

756    **Appendix.** Abbreviations used in the main text.
757
758    **SA:** sulfuric acid
759    **DMA:** dimethylamine
760    **ACDC:** Atmospheric Cluster Dynamic Code
761    **DB**: DLPNO-CCSD(T)/aug-cc-pVTZ//ωB97X-D/6-311++G(3df,3pd) level of theory
762    **RM**: RI-CC2/aug-cc-pV(T+d)Z//M06-2X/6–311++G(3df,3pd) level of theory
763    **CE:** simplification in cluster evaporations (only $(SA)_k(DMA)_k$ ($k$ = 1-4) and
764    $(SA)_2(DMA)_1$ clusters are considered)
765    **CN**: simplification in cluster number (clusters larger than $(SA)_1(DMA)_1$ are regarded
766    stable with no evaporation)
767    **BC:** simplification in boundary conditions ($(SA)_4(DMA)_4$ cluster is set as the only
768    terminal cluster in calculating particle formation rates)
769    **SF**: sticking factor used in collision process
770    **Dynamic_Sim:** a reported cluster-dynamic based parameterization incorporating
771    simplifications of CE, CN and BC.
772    $J_{1.4}$: particle formation rate at 1.4 nm
773    $R$: a parameter to quantify the differences in simulating $J_{1.4}$ among different cluster
774    dynamics-based parameterizations compared to the base-case ACDC_DB
775

**Code and data availability.** The data and code used in this study are available upon request from the corresponding author.

**Author contributions**. JS, BZ, and SW designed the research; AN and XZ collected the quantum chemistry calculation data; JS performed the ACDC and WRF-Chem/R2D-VBS simulations; YL, RC, and JJ collected the observational data. JS, BZ, and SW analyzed the data; RC, DG, JJ, YG, MS, BC, and HH presented important suggestions for the paper; JS, BZ, and SW wrote the paper with input from all co-authors.

**Competing interests.** At least one of the (co-)authors is a member of the editorial board of Atmospheric Chemistry and Physics.

**Acknowledgements.** This study was supported by the National Natural Science Foundation of China (22188102 and 42275110) and Samsung $PM_{2.5}$ SRP.

**Financial support.** Financial support from National Natural Science Foundation of China (22188102 and 42275110) and Samsung $PM_{2.5}$ SRP.

**REFERENCES**

Almeida, J., Schobesberger, S., Kurten, A., Ortega, I. K., Kupiainen-Maatta, O., Praplan, A. P., Adamov, A., Amorim, A., Bianchi, F., Breitenlechner, M., David, A., Dommen, J., Donahue, N. M., Downard, A., Dunne, E., Duplissy, J., Ehrhart, S., Flagan, R. C., Franchin, A., Guida, R., Hakala, J., Hansel, A., Heinritzi, M., Henschel, H., Jokinen, T., Junninen, H., Kajos, M., Kangasluoma, J., Keskinen, H., Kupc, A., Kurten, T., Kvashin, A. N., Laaksonen, A., Lehtipalo, K., Leiminger, M., Leppa, J., Loukonen, V., Makhmutov, V., Mathot, S., McGrath, M. J., Nieminen, T., Olenius, T., Onnela, A., Petaja, T., Riccobono, F., Riipinen, I., Rissanen, M., Rondo, L., Ruuskanen, T., Santos, F. D., Sarnela, N., Schallhart, S., Schnitzhofer, R., Seinfeld, J. H., Simon, M., Sipila, M., Stozhkov, Y., Stratmann, F., Tome, A., Trostl, J., Tsagkogeorgas, G., Vaattovaara, P., Viisanen, Y., Virtanen, A., Vrtala, A., Wagner, P. E., Weingartner, E., Wex, H., Williamson, C., Wimmer, D., Ye, P., Yli-Juuti, T., Carslaw, K. S., Kulmala, M., Curtius, J., Baltensperger, U., Worsnop, D. R., Vehkamaki, H., and Kirkby, J.: Molecular understanding of sulphuric acid-amine particle nucleation in the atmosphere, Nature, 502, 359-363, 10.1038/nature12663, 2013.

Baranizadeh, E., Murphy, B. N., Julin, J., Falahat, S., Reddington, C. L., Arola, A., Ahlm, L., Mikkonen, S., Fountoukis, C., Patoulias, D., Minikin, A., Hamburger, T., Laaksonen, A., Pandis, S. N., Vehkamäki, H., Lehtinen, K. E. J., and Riipinen, I.: Implementation of state-of-the-art ternary new-particle formation scheme to the regional chemical transport model PMCAMx-UF in Europe, Geoscientific Model Development, 9, 2741-2754, 10.5194/gmd-9-2741-2016, 2016.

Bergman, T., Laaksonen, A., Korhonen, H., Malila, J., Dunne, E. M., Mielonen, T., Lehtinen, K. E. J., Kühn, T., Arola, A., and Kokkola, H.: Geographical and diurnal features of amine‐enhanced boundary layer nucleation, Journal of Geophysical Research: Atmospheres, 120, 9606-9624, 10.1002/2015jd023181, 2015.

Besel, V., Kubecka, J., Kurten, T., and Vehkamaki, H.: Impact of Quantum Chemistry Parameter Choices and Cluster Distribution Model Settings on Modeled Atmospheric Particle Formation Rates, J Phys Chem A, 124, 5931-5943, 10.1021/acs.jpca.0c03984, 2020.

Brasseur GP, Jacob DJ. Model Equations and Numerical Approaches. In: Modeling of Atmospheric Chemistry. Cambridge University Press; 2017:84-204.

Cai, R. and Jiang, J.: A new balance formula to estimate new particle formation rate: reevaluating the effect of coagulation scavenging, Atmospheric Chemistry and Physics, 17, 12659-12675, 10.5194/acp-17-12659-2017, 2017.

Cai, R., Yin, R., Li, X., Xie, H.-B., Yang, D., Kerminen, V.-M., Smith, J. N., Ma, Y., Hao, J., Chen, J., Kulmala, M., Zheng, J., Jiang, J., and Elm, J.: Significant contributions of trimethylamine to sulfuric acid nucleation in polluted

environments, npj Climate and Atmospheric Science, 6, 10.1038/s41612-023-00405-3, 2023.

Cai, R., Yan, C., Yang, D., Yin, R., Lu, Y., Deng, C., Fu, Y., Ruan, J., Li, X., Kontkanen, J., Zhang, Q., Kangasluoma, J., Ma, Y., Hao, J., Worsnop, D. R., Bianchi, F., Paasonen, P., Kerminen, V.-M., Liu, Y., Wang, L., Zheng, J., Kulmala, M., and Jiang, J.: Sulfuric acid–amine nucleation in urban Beijing, Atmospheric Chemistry and Physics, 21, 2457-2468, 10.5194/acp-21-2457-2021, 2021.

Chu, B., Kerminen, V.-M., Bianchi, F., Yan, C., Petäjä, T., and Kulmala, M.: Atmospheric new particle formation in China, Atmospheric Chemistry and Physics, 19, 115-138, 10.5194/acp-19-115-2019, 2019.

Croft, B., Wentworth, G. R., Martin, R. V., Leaitch, W. R., Murphy, J. G., Murphy, B. N., Kodros, J. K., Abbatt, J. P. D., and Pierce, J. R.: Contribution of Arctic seabird-colony ammonia to atmospheric particles and cloud-albedo radiative effect, Nature Communications, 7, 10.1038/ncomms13444, 2016.

Dal Maso, M., Hyvärinen, A., Komppula, M., Tunved, P., Kerminen, V.-M., Lihavainen, H., Viisanen, Y., Hansson, H.-C., and Kulmala, M.: Annual and interannual variation in boreal forest aerosol particle number and volume concentration and their connection to particle formation, Tellus B: Chemical and Physical Meteorology, 60, 10.1111/j.1600-0889.2008.00366.x, 2008.

Deng, C., Fu, Y., Dada, L., Yan, C., Cai, R., Yang, D., Zhou, Y., Yin, R., Lu, Y., Li, X., Qiao, X., Fan, X., Nie, W., Kontkanen, J., Kangasluoma, J., Chu, B., Ding, A., Kerminen, V. M., Paasonen, P., Worsnop, D. R., Bianchi, F., Liu, Y., Zheng, J., Wang, L., Kulmala, M., and Jiang, J.: Seasonal Characteristics of New Particle Formation and Growth in Urban Beijing, Environ Sci Technol, 54, 8547-8557, 10.1021/acs.est.0c00808, 2020.

Dunne, E. M., Gordon, H., Kurten, A., Almeida, J., Duplissy, J., Williamson, C., Ortega, I. K., Pringle, K. J., Adamov, A., Baltensperger, U., Barmet, P., Benduhn, F., Bianchi, F., Breitenlechner, M., Clarke, A., Curtius, J., Dommen, J., Donahue, N. M., Ehrhart, S., Flagan, R. C., Franchin, A., Guida, R., Hakala, J., Hansel, A., Heinritzi, M., Jokinen, T., Kangasluoma, J., Kirkby, J., Kulmala, M., Kupc, A., Lawler, M. J., Lehtipalo, K., Makhmutov, V., Mann, G., Mathot, S., Merikanto, J., Miettinen, P., Nenes, A., Onnela, A., Rap, A., Reddington, C. L., Riccobono, F., Richards, N. A., Rissanen, M. P., Rondo, L., Sarnela, N., Schobesberger, S., Sengupta, K., Simon, M., Sipila, M., Smith, J. N., Stozkhov, Y., Tome, A., Trostl, J., Wagner, P. E., Wimmer, D., Winkler, P. M., Worsnop, D. R., and Carslaw, K. S.: Global atmospheric particle formation from CERN CLOUD measurements, Science, 354, 1119-1124, 10.1126/science.aaf2649, 2016.

Elm, J., Bilde, M., and Mikkelsen, K. V.: Assessment of binding energies of atmospherically relevant clusters, Phys Chem Chem Phys, 15, 16442-16445, 10.1039/c3cp52616j, 2013.

880     Elm, J., Kubečka, J., Besel, V., Jääskeläinen, M. J., Halonen, R., Kurtén, T., and
881          Vehkamäki, H.: Modeling the formation and growth of atmospheric molecular
882          clusters: A review, Journal of Aerosol Science, 149,
883          10.1016/j.jaerosci.2020.105621, 2020.
884     Gao, D., Zhao, B., Wang, S. X., Shen, J. W., Wang, Y., Zhou, C., Jiang, J. K., Wu, Q.
885          R., Li, S. Y., Sun, Y. S., He, Y. C., Zhu, Y., and Jiang, Z.: Distinct $PM_{2.5}$-
886          Related Near-Term Climate Penalties Induced by Different Clean Air
887          Measures in China, Geophysical Research Letters, 51, 10.1029/2024gl108204,
888          2024.
889     Gordon, H., Sengupta, K., Rap, A., Duplissy, J., Frege, C., Williamson, C., Heinritzi,
890          M., Simon, M., Yan, C., Almeida, J., Trostl, J., Nieminen, T., Ortega, I. K.,
891          Wagner, R., Dunne, E. M., Adamov, A., Amorim, A., Bernhammer, A. K.,
892          Bianchi, F., Breitenlechner, M., Brilke, S., Chen, X., Craven, J. S., Dias, A.,
893          Ehrhart, S., Fischer, L., Flagan, R. C., Franchin, A., Fuchs, C., Guida, R.,
894          Hakala, J., Hoyle, C. R., Jokinen, T., Junninen, H., Kangasluoma, J., Kim, J.,
895          Kirkby, J., Krapf, M., Kurten, A., Laaksonen, A., Lehtipalo, K., Makhmutov,
896          V., Mathot, S., Molteni, U., Monks, S. A., Onnela, A., Perakyla, O., Piel, F.,
897          Petaja, T., Praplan, A. P., Pringle, K. J., Richards, N. A., Rissanen, M. P.,
898          Rondo, L., Sarnela, N., Schobesberger, S., Scott, C. E., Seinfeld, J. H.,
899          Sharma, S., Sipila, M., Steiner, G., Stozhkov, Y., Stratmann, F., Tome, A.,
900          Virtanen, A., Vogel, A. L., Wagner, A. C., Wagner, P. E., Weingartner, E.,
901          Wimmer, D., Winkler, P. M., Ye, P., Zhang, X., Hansel, A., Dommen, J.,
902          Donahue, N. M., Worsnop, D. R., Baltensperger, U., Kulmala, M., Curtius, J.,
903          and Carslaw, K. S.: Reduced anthropogenic aerosol radiative forcing caused
904          by biogenic new particle formation, Proc Natl Acad Sci U S A, 113, 12053-
905          12058, 10.1073/pnas.1602360113, 2016.
906     Guenther, A., Karl, T., Harley, P., Wiedinmyer, C., Palmer, P. I., and Geron, C.:
907          Estimates of global terrestrial isoprene emissions using MEGAN (Model of
908          Emissions of Gases and Aerosols from Nature), Atmos. Chem. Phys., 6, 3181-
909          3210, 10.5194/acp-6-3181-2006, 2006.
910     He, X. C., Tham, Y. J., Dada, L., Wang, M., Finkenzeller, H., Stolzenburg, D., Iyer, S.,
911          Simon, M., Kurten, A., Shen, J., Rorup, B., Rissanen, M., Schobesberger, S.,
912          Baalbaki, R., Wang, D. S., Koenig, T. K., Jokinen, T., Sarnela, N., Beck, L. J.,
913          Almeida, J., Amanatidis, S., Amorim, A., Ataei, F., Baccarini, A., Bertozzi, B.,
914          Bianchi, F., Brilke, S., Caudillo, L., Chen, D., Chiu, R., Chu, B., Dias, A.,
915          Ding, A., Dommen, J., Duplissy, J., El Haddad, I., Gonzalez Carracedo, L.,
916          Granzin, M., Hansel, A., Heinritzi, M., Hofbauer, V., Junninen, H.,
917          Kangasluoma, J., Kemppainen, D., Kim, C., Kong, W., Krechmer, J. E.,
918          Kvashin, A., Laitinen, T., Lamkaddam, H., Lee, C. P., Lehtipalo, K.,
919          Leiminger, M., Li, Z., Makhmutov, V., Manninen, H. E., Marie, G., Marten,
920          R., Mathot, S., Mauldin, R. L., Mentler, B., Mohler, O., Muller, T., Nie, W.,
921          Onnela, A., Petaja, T., Pfeifer, J., Philippov, M., Ranjithkumar, A., Saiz-Lopez,

A., Salma, I., Scholz, W., Schuchmann, S., Schulze, B., Steiner, G., Stozhkov, Y., Tauber, C., Tome, A., Thakur, R. C., Vaisanen, O., Vazquez-Pufleau, M., Wagner, A. C., Wang, Y., Weber, S. K., Winkler, P. M., Wu, Y., Xiao, M., Yan, C., Ye, Q., Ylisirnio, A., Zauner-Wieczorek, M., Zha, Q., Zhou, P., Flagan, R. C., Curtius, J., Baltensperger, U., Kulmala, M., Kerminen, V. M., Kurten, T., Donahue, N. M., Volkamer, R., Kirkby, J., Worsnop, D. R., and Sipila, M.: Role of iodine oxoacids in atmospheric aerosol nucleation, Science, 371, 589-595, 10.1126/science.abe0298, 2021.

Jen, C. N., Hanson, D. R., and McMurry, P. H.: Toward Reconciling Measurements of Atmospherically Relevant Clusters by Chemical Ionization Mass Spectrometry and Mobility Classification/Vapor Condensation, Aerosol Science and Technology, 49, i-iii, 10.1080/02786826.2014.1002602, 2014.

Julin, J., Murphy, B. N., Patoulias, D., Fountoukis, C., Olenius, T., Pandis, S. N., and Riipinen, I.: Impacts of Future European Emission Reductions on Aerosol Particle Number Concentrations Accounting for Effects of Ammonia, Amines, and Organic Species, Environ Sci Technol, 52, 692-700, 10.1021/acs.est.7b05122, 2018.

Kirkby, J., Curtius, J., Almeida, J., Dunne, E., Duplissy, J., Ehrhart, S., Franchin, A., Gagne, S., Ickes, L., Kurten, A., Kupc, A., Metzger, A., Riccobono, F., Rondo, L., Schobesberger, S., Tsagkogeorgas, G., Wimmer, D., Amorim, A., Bianchi, F., Breitenlechner, M., David, A., Dommen, J., Downard, A., Ehn, M., Flagan, R. C., Haider, S., Hansel, A., Hauser, D., Jud, W., Junninen, H., Kreissl, F., Kvashin, A., Laaksonen, A., Lehtipalo, K., Lima, J., Lovejoy, E. R., Makhmutov, V., Mathot, S., Mikkila, J., Minginette, P., Mogo, S., Nieminen, T., Onnela, A., Pereira, P., Petaja, T., Schnitzhofer, R., Seinfeld, J. H., Sipila, M., Stozhkov, Y., Stratmann, F., Tome, A., Vanhanen, J., Viisanen, Y., Vrtala, A., Wagner, P. E., Walther, H., Weingartner, E., Wex, H., Winkler, P. M., Carslaw, K. S., Worsnop, D. R., Baltensperger, U., and Kulmala, M.: Role of sulphuric acid, ammonia and galactic cosmic rays in atmospheric aerosol nucleation, Nature, 476, 429-433, 10.1038/nature10343, 2011.

Kirkby, J., Duplissy, J., Sengupta, K., Frege, C., Gordon, H., Williamson, C., Heinritzi, M., Simon, M., Yan, C., Almeida, J., Trostl, J., Nieminen, T., Ortega, I. K., Wagner, R., Adamov, A., Amorim, A., Bernhammer, A. K., Bianchi, F., Breitenlechner, M., Brilke, S., Chen, X., Craven, J., Dias, A., Ehrhart, S., Flagan, R. C., Franchin, A., Fuchs, C., Guida, R., Hakala, J., Hoyle, C. R., Jokinen, T., Junninen, H., Kangasluoma, J., Kim, J., Krapf, M., Kurten, A., Laaksonen, A., Lehtipalo, K., Makhmutov, V., Mathot, S., Molteni, U., Onnela, A., Perakyla, O., Piel, F., Petaja, T., Praplan, A. P., Pringle, K., Rap, A., Richards, N. A., Riipinen, I., Rissanen, M. P., Rondo, L., Sarnela, N., Schobesberger, S., Scott, C. E., Seinfeld, J. H., Sipila, M., Steiner, G., Stozhkov, Y., Stratmann, F., Tome, A., Virtanen, A., Vogel, A. L., Wagner, A. C., Wagner, P. E., Weingartner, E., Wimmer, D., Winkler, P. M., Ye, P., Zhang,

X., Hansel, A., Dommen, J., Donahue, N. M., Worsnop, D. R., Baltensperger, U., Kulmala, M., Carslaw, K. S., and Curtius, J.: Ion-induced nucleation of pure biogenic particles, Nature, 533, 521-526, 10.1038/nature17953, 2016.

Kulmala, M., Lehtinen, K. E. J., and Laaksonen, A.: Cluster activation theory as an explanation of the linear dependence between formation rate of 3nm particles and sulphuric acid concentration, Atmospheric Chemistry and Physics, 6, 787-793, DOI 10.5194/acp-6-787-2006, 2006.

Kürten, A., Li, C., Bianchi, F., Curtius, J., Dias, A., Donahue, N. M., Duplissy, J., Flagan, R. C., Hakala, J., Jokinen, T., Kirkby, J., Kulmala, M., Laaksonen, A., Lehtipalo, K., Makhmutov, V., Onnela, A., Rissanen, M. P., Simon, M., Sipilä, M., Stozhkov, Y., Tröstl, J., Ye, P., and McMurry, P. H.: New particle formation in the sulfuric acid–dimethylamine–water system: reevaluation of CLOUD chamber measurements and comparison to an aerosol nucleation and growth model, Atmospheric Chemistry and Physics, 18, 845-863, 10.5194/acp-18-845-2018, 2018.

Lehtinen, K. E. J., Dal Maso, M., Kulmala, M., and Kerminen, V. M.: Estimating nucleation rates from apparent particle formation rates and vice versa: Revised formulation of the Kerminen-Kulmala equation, Journal of Aerosol Science, 38, 988-994, 10.1016/j.jaerosci.2007.06.009, 2007.

Li, C., Zhao, Y., Li, Z., Liu, L., Zhang, X., Zheng, J., Kerminen, V.-M., Kulmala, M., Jiang, J., Cai, R., and Xiao, H.: The dependence of new particle formation rates on the interaction between cluster growth, evaporation, and condensation sink, Environmental Science: Atmospheres, 3, 168-181, 10.1039/d2ea00066k, 2023a.

Li, H., Ning, A., Zhong, J., Zhang, H., Liu, L., Zhang, Y., Zhang, X., Zeng, X. C., and He, H.: Influence of atmospheric conditions on sulfuric acid-dimethylamine-ammonia-based new particle formation, Chemosphere, 245, 125554, 10.1016/j.chemosphere.2019.125554, 2020.

Li, M., Zhang, Q., Kurokawa, J., Woo, J. H., He, K. B., Lu, Z. F., Ohara, T., Song, Y., Streets, D. G., Carmichael, G. R., Cheng, Y. F., Hong, C. P., Huo, H., Jiang, X. J., Kang, S. C., Liu, F., Su, H., and Zheng, B.: MIX: a mosaic Asian anthropogenic emission inventory under the international collaboration framework of the MICS-Asia and HTAP, Atmospheric Chemistry and Physics, 17, 935-963, 10.5194/acp-17-935-2017, 2017.

Li, S., Wang, S., Wu, Q., Zhang, Y., Ouyang, D., Zheng, H., Han, L., Qiu, X., Wen, Y., Liu, M., Jiang, Y., Yin, D., Liu, K., Zhao, B., Zhang, S., Wu, Y., and Hao, J.: Emission trends of air pollutants and CO2 in China from 2005 to 2021, Earth System Science Data, 15, 2279-2294, 10.5194/essd-15-2279-2023, 2023b.

Li, Y., Shen, J., Zhao, B., Cai, R., Wang, S., Gao, Y., Shrivastava, M., Gao, D., Zheng, J., Kulmala, M., and Jiang, J.: A dynamic parameterization of sulfuric acid–dimethylamine nucleation and its application in three-dimensional modeling, Atmospheric Chemistry and Physics, 23, 8789-8804, 10.5194/acp-23-8789-

1006      2023, 2023c.

1007    Liu, L., Yu, F., Tu, K., Yang, Z., and Zhang, X.: Influence of atmospheric conditions
1008         on the role of trifluoroacetic acid in atmospheric sulfuric acid–dimethylamine
1009         nucleation, Atmospheric Chemistry and Physics, 21, 6221-6230, 10.5194/acp-
1010         21-6221-2021, 2021.

1011    Liu, L., Zhong, J., Vehkamaki, H., Kurten, T., Du, L., Zhang, X., Francisco, J. S., and
1012         Zeng, X. C.: Unexpected quenching effect on new particle formation from the
1013         atmospheric reaction of methanol with SO3, Proc Natl Acad Sci U S A, 116,
1014         24966-24971, 10.1073/pnas.1915459116, 2019.

1015    Lu, Y., Liu, L., Ning, A., Yang, G., Liu, Y., Kurtén, T., Vehkamäki, H., Zhang, X., and
1016         Wang, L.: Atmospheric Sulfuric Acid‐Dimethylamine Nucleation Enhanced
1017         by Trifluoroacetic Acid, Geophysical Research Letters, 47,
1018         10.1029/2019gl085627, 2020.

1019    Ma, F., Xie, H. B., Elm, J., Shen, J., Chen, J., and Vehkamaki, H.: Piperazine
1020         Enhancing Sulfuric Acid-Based New Particle Formation: Implications for the
1021         Atmospheric Fate of Piperazine, Environ Sci Technol, 53, 8785-8795,
1022         10.1021/acs.est.9b02117, 2019.

1023    McGrath, M. J., Olenius, T., Ortega, I. K., Loukonen, V., Paasonen, P., Kurtén, T.,
1024         Kulmala, M., and Vehkamäki, H.: Atmospheric Cluster Dynamics Code: a
1025         flexible method for solution of the birth-death equations, Atmospheric
1026         Chemistry and Physics, 12, 2345-2355, 10.5194/acp-12-2345-2012, 2012.

1027    Myllys, N., Chee, S., Olenius, T., Lawler, M., and Smith, J.: Molecular-Level
1028         Understanding of Synergistic Effects in Sulfuric Acid-Amine-Ammonia
1029         Mixed Clusters, J Phys Chem A, 123, 2420-2425, 10.1021/acs.jpca.9b00909,
1030         2019.

1031    Ning, A. and Zhang, X.: The synergistic effects of methanesulfonic acid (MSA) and
1032         methanesulfinic acid (MSIA) on marine new particle formation, Atmospheric
1033         Environment, 269, 10.1016/j.atmosenv.2021.118826, 2022.

1034    Ning, A., Liu, L., Ji, L., and Zhang, X.: Molecular-level nucleation mechanism of
1035         iodic acid and methanesulfonic acid, Atmospheric Chemistry and Physics, 22,
1036         6103-6114, 10.5194/acp-22-6103-2022, 2022.

1037    Ning, A., Zhang, H., Zhang, X., Li, Z., Zhang, Y., Xu, Y., and Ge, M.: A molecular-
1038         scale study on the role of methanesulfinic acid in marine new particle
1039         formation, Atmospheric Environment, 227, 10.1016/j.atmosenv.2020.117378,
1040         2020.

1041    Ning, A., Shen, J., Zhao, B., Wang, S., Cai, R., Jiang, J. Yan, C., Fu, X., Zhang, Y., Li,
1042         J., Ouyang, D., Sun, Y., Saiz-Lopez, A., Francisco, J., and Zhang, X.:
1043         Overlooked significance of iodic acid in new particle formation in the
1044         continental atmosphere, Proc Natl Acad Sci U S A, 2024. In press~~Preparation~~.

1045    Olenius, T., Kupiainen-Maatta, O., Ortega, I. K., Kurten, T., and Vehkamaki, H.: Free
1046         energy barrier in the growth of sulfuric acid-ammonia and sulfuric acid-
1047         dimethylamine clusters, J Chem Phys, 139, 084312, 10.1063/1.4819024, 2013.

Olenius, T., Halonen, R., Kurtén, T., Henschel, H., Kupiainen - Määttä, O., Ortega, I. K., Jen, C. N., Vehkamäki, H., and Riipinen, I.: New particle formation from sulfuric acid and amines: Comparison of monomethylamine, dimethylamine, and trimethylamine, Journal of Geophysical Research: Atmospheres, 122, 7103-7118, 10.1002/2017jd026501, 2017.

Olenius, T. and Roldin, P.: Role of gas-molecular cluster-aerosol dynamics in atmospheric new-particle formation, Sci Rep, 12, 10135, 10.1038/s41598-022-14525-y, 2022.

Olin, M., Patoulias, D., Kuuluvainen, H., Niemi, J. V., Rönkkö, T., Pandis, S. N., Riipinen, I., and Dal Maso, M.: Contribution of traffic-originated nanoparticle emissions to regional and local aerosol levels, Atmospheric Chemistry and Physics, 22, 1131-1148, 10.5194/acp-22-1131-2022, 2022.

Ortega, I. K., Kupiainen, O., Kurtén, T., Olenius, T., Wilkman, O., McGrath, M. J., Loukonen, V., and Vehkamäki, H.: From quantum chemical formation free energies to evaporation rates, Atmospheric Chemistry and Physics, 12, 225-235, 10.5194/acp-12-225-2012, 2012.

Riccobono, F., Schobesberger, S., Scott, C. E., Dommen, J., Ortega, I. K., Rondo, L., Almeida, J., Amorim, A., Bianchi, F., Breitenlechner, M., David, A., Downard, A., Dunne, E. M., Duplissy, J., Ehrhart, S., Flagan, R. C., Franchin, A., Hansel, A., Junninen, H., Kajos, M., Keskinen, H., Kupc, A., Kurten, A., Kvashin, A. N., Laaksonen, A., Lehtipalo, K., Makhmutov, V., Mathot, S., Nieminen, T., Onnela, A., Petaja, T., Praplan, A. P., Santos, F. D., Schallhart, S., Seinfeld, J. H., Sipila, M., Spracklen, D. V., Stozhkov, Y., Stratmann, F., Tome, A., Tsagkogeorgas, G., Vaattovaara, P., Viisanen, Y., Vrtala, A., Wagner, P. E., Weingartner, E., Wex, H., Wimmer, D., Carslaw, K. S., Curtius, J., Donahue, N. M., Kirkby, J., Kulmala, M., Worsnop, D. R., and Baltensperger, U.: Oxidation Products of Biogenic Emissions Contribute to Nucleation of Atmospheric Particles, Science, 344, 717-721, 10.1126/science.1243527, 2014.

Semeniuk, K. and Dastoor, A.: Current state of aerosol nucleation parameterizations for air-quality and climate modeling, Atmospheric Environment, 179, 77-106, 10.1016/j.atmosenv.2018.01.039, 2018.

Stolzenburg, D., Simon, M., Ranjithkumar, A., Kürten, A., Lehtipalo, K., Gordon, H., Ehrhart, S., Finkenzeller, H., Pichelstorfer, L., Nieminen, T., He, X.-C., Brilke, S., Xiao, M., Amorim, A., Baalbaki, R., Baccarini, A., Beck, L., Bräkling, S., Caudillo Murillo, L., Chen, D., Chu, B., Dada, L., Dias, A., Dommen, J., Duplissy, J., El Haddad, I., Fischer, L., Gonzalez Carracedo, L., Heinritzi, M., Kim, C., Koenig, T. K., Kong, W., Lamkaddam, H., Lee, C. P., Leiminger, M., Li, Z., Makhmutov, V., Manninen, H. E., Marie, G., Marten, R., Müller, T., Nie, W., Partoll, E., Petäjä, T., Pfeifer, J., Philippov, M., Rissanen, M. P., Rörup, B., Schobesberger, S., Schuchmann, S., Shen, J., Sipilä, M., Steiner, G., Stozhkov, Y., Tauber, C., Tham, Y. J., Tomé, A., Vazquez-Pufleau, M.,

Wagner, A. C., Wang, M., Wang, Y., Weber, S. K., Wimmer, D., Wlasits, P. J., Wu, Y., Ye, Q., Zauner-Wieczorek, M., Baltensperger, U., Carslaw, K. S., Curtius, J., Donahue, N. M., Flagan, R. C., Hansel, A., Kulmala, M., Lelieveld, J., Volkamer, R., Kirkby, J., and Winkler, P. M.: Enhanced growth rate of atmospheric particles from sulfuric acid, Atmospheric Chemistry and Physics, 20, 7359-7372, 10.5194/acp-20-7359-2020, 2020.

Svenhag, C., Sporre, M. K., Olenius, T., Yazgi, D., Blichner, S. M., Nieradzik, L. P., and Roldin, P.: Implementing detailed nucleation predictions in the Earth system model EC-Earth3.3.4: sulfuric acid-ammonia nucleation, EGUsphere [preprint], https://doi.org/10.5194/egusphere-2023-2665, 2024.

Thomas, J. M., He, S., Larriba-Andaluz, C., DePalma, J. W., Johnston, M. V., and Hogan, C. J., Jr.: Ion mobility spectrometry-mass spectrometry examination of the structures, stabilities, and extents of hydration of dimethylamine-sulfuric acid clusters, Phys Chem Chem Phys, 18, 22962-22972, 10.1039/c6cp03432b, 2016.

Xiao, M., Hoyle, C. R., Dada, L., Stolzenburg, D., Kürten, A., Wang, M., Lamkaddam, H., Garmash, O., Mentler, B., Molteni, U., Baccarini, A., Simon, M., He, X.-C., Lehtipalo, K., Ahonen, L. R., Baalbaki, R., Bauer, P. S., Beck, L., Bell, D., Bianchi, F., Brilke, S., Chen, D., Chiu, R., Dias, A., Duplissy, J., Finkenzeller, H., Gordon, H., Hofbauer, V., Kim, C., Koenig, T. K., Lampilahti, J., Lee, C. P., Li, Z., Mai, H., Makhmutov, V., Manninen, H. E., Marten, R., Mathot, S., Mauldin, R. L., Nie, W., Onnela, A., Partoll, E., Petäjä, T., Pfeifer, J., Pospisilova, V., Quéléver, L. L. J., Rissanen, M., Schobesberger, S., Schuchmann, S., Stozhkov, Y., Tauber, C., Tham, Y. J., Tomé, A., Vazquez-Pufleau, M., Wagner, A. C., Wagner, R., Wang, Y., Weitz, L., Wimmer, D., Wu, Y., Yan, C., Ye, P., Ye, Q., Zha, Q., Zhou, X., Amorim, A., Carslaw, K., Curtius, J., Hansel, A., Volkamer, R., Winkler, P. M., Flagan, R. C., Kulmala, M., Worsnop, D. R., Kirkby, J., Donahue, N. M., Baltensperger, U., El Haddad, I., and Dommen, J.: The driving factors of new particle formation and growth in the polluted boundary layer, Atmospheric Chemistry and Physics, 21, 14275-14291, 10.5194/acp-21-14275-2021, 2021.

Xie, H. B., Elm, J., Halonen, R., Myllys, N., Kurten, T., Kulmala, M., and Vehkamaki, H.: Atmospheric Fate of Monoethanolamine: Enhancing New Particle Formation of Sulfuric Acid as an Important Removal Process, Environ Sci Technol, 51, 8422-8431, 10.1021/acs.est.7b02294, 2017.

Yang, S., Liu, Z., Clusius, P. S., Liu, Y., Zou, J., Yang, Y., Zhao, S., Zhang, G., Xu, Z., Ma, Z., Yang, Y., Sun, J., Pan, Y., Ji, D., Hu, B., Yan, C., Boy, M., Kulmala, M., and Wang, Y.: Chemistry of new particle formation and growth events during wintertime in suburban area of Beijing: Insights from highly polluted atmosphere, Atmospheric Research, 255, 10.1016/j.atmosres.2021.105553, 2021.

Yao, L., Garmash, O., Bianchi, F., Zheng, J., Yan, C., Kontkanen, J., Junninen, H.,

Mazon, S. B., Ehn, M., Paasonen, P., Sipila, M., Wang, M., Wang, X., Xiao, S., Chen, H., Lu, Y., Zhang, B., Wang, D., Fu, Q., Geng, F., Li, L., Wang, H., Qiao, L., Yang, X., Chen, J., Kerminen, V. M., Petaja, T., Worsnop, D. R., Kulmala, M., and Wang, L.: Atmospheric new particle formation from sulfuric acid and amines in a Chinese megacity, Science, 361, 278-281, 10.1126/science.aao4839, 2018.

Yazgi, D. and Olenius, T.: J-GAIN v1.1: a flexible tool to incorporate aerosol formation rates obtained by molecular models into large-scale models, Geoscientific Model Development, 16, 5237-5249, 10.5194/gmd-16-5237-2023, 2023.

Yu, F.: Ion-mediated nucleation in the atmosphere: Key controlling parameters, implications, and look-up table, Journal of Geophysical Research, 115, 10.1029/2009jd012630, 2010.

Zhao, B., Shrivastava, M., Donahue, N. M., Gordon, H., Schervish, M., Shilling, J. E., Zaveri, R. A., Wang, J., Andreae, M. O., Zhao, C., Gaudet, B., Liu, Y., Fan, J., and Fast, J. D.: High concentration of ultrafine particles in the Amazon free troposphere produced by organic new particle formation, Proc Natl Acad Sci U S A, 117, 25344-25351, 10.1073/pnas.2006716117, 2020.

Zheng, H. T., Cai, S. Y., Wang, S. X., Zhao, B., Chang, X., and Hao, J. M.: Development of a unit-based industrial emission inventory in the Beijing-Tianjin-Hebei region and resulting improvement in air quality modeling, Atmospheric Chemistry and Physics, 19, 3447-3462, 10.5194/acp-19-3447-2019, 2019.

Zhu, S., Yan, C., Zheng, J., Chen, C., Ning, H., Yang, D., Wang, M., Ma, Y., Zhan, J., Hua, C., Yin, R., Li, Y., Liu, Y., Jiang, J., Yao, L., Wang, L., Kulmala, M., and Worsnop, D. R.: Observation and Source Apportionment of Atmospheric Alkaline Gases in Urban Beijing, Environ Sci Technol, 56, 17545-17555, 10.1021/acs.est.2c03584, 2022.